2. EXPLANATORY NOTES[1]

Shipboard Scientific Party[2]

INTRODUCTION

This chapter explains the techniques and procedures used during Leg 195 to help document the basis for our preliminary scientific conclusions and to provide the interested investigator with the information needed to select samples for further analysis. This information concerns only shipboard operations and analyses described in the site reports in the *Initial Reports* volume of the Leg 195 *Proceedings of the Ocean Drilling Program*. Methods used by various investigators for shore-based analyses of Leg 195 data will be described in the individual scientific contributions published in the *Scientific Results* volume and in publications in various professional journals.

Authorship of Site Chapters

The separate sections of the site chapters were written by the following shipboard scientists, and the summary chapter is derived from all their contributions (authors are listed in alphabetical order; no seniority is implied):

Summary: Salisbury, Shinohara
Background and Objectives: Fryer, Salisbury, Shinohara, Wei
Operations: Richter, Storms
Lithostratigraphy: Diekmann, Januszczak
Petrology: D'Antonio, Fryer, Kristensen, Lockwood, Savov
Structural Geology: Lockwood
Biostratigraphy: Su, Wei
Paleomagnetism: Richter
Geochemistry: Komor, Mottl
Physical Properties: Dean, Hammon, Hart
Downhole Measurements: Barr, Gaillot

Microbiology: Moyer
Borehole Instrumentation: Araki, Edwards, Nakahigashi, Schroeder, Shinohara, Yamada

Use of "Ma" vs. "m.y."

1. The term *Ma* is equivalent to and replaces m.y.B.P. (million years before present); for example, 35–40 Ma.
2. The term *m.y.* is used in sentences such as "... for 5 m.y. in the early Miocene."

Drilling Characteristics

Information concerning sedimentary stratification in uncored or unrecovered intervals may be inferred from seismic data, wireline logging results, and examination of the behavior of the drill string, as observed and recorded on the drilling platform. Typically, the harder a layer, the slower and more difficult it is to penetrate. Because a number of other factors may determine the rate of penetration, it is not always possible to relate drilling time directly to the hardness of the layers. Bit weight and revolutions per minute, recorded with a new acquisition program (Fusion), also influence the penetration rate.

Drilling Deformation

When cores are split, many show signs of significant sediment disturbance, including the concave-downward appearance of originally horizontal bedding, haphazard mixing of lumps of different lithologies (mainly at the tops of cores), fluidization, and flow-in. Core deformation may also occur during retrieval, because of changes in pressure and temperature as the core is raised, and during cutting and core handling on deck.

Shipboard Scientific Procedures

Numbering of Sites, Holes, Cores, and Samples

Ocean Drilling Program (ODP) drill sites are numbered consecutively and refer to one or more holes drilled while the ship was positioned over one acoustic beacon. Multiple holes may be drilled at a single site by pulling the drill pipe above the seafloor (out of the hole), moving the ship some distance from the previous hole, and then drilling another hole.

For all ODP drill sites, a letter suffix distinguishes each hole drilled at the same site. The first hole drilled is assigned the site number modified by the suffix "A," the second hole takes the site number and suffix "B," and so forth. Note that this procedure differs slightly from that used by DSDP (Sites 1 through 624) but prevents ambiguity between site- and hole-number designations. It is important to distinguish between holes drilled at a site because recovered sediments or rocks from different holes usually do not come from exactly equivalent positions in the stratigraphic column.

The cored interval is measured in meters below seafloor (mbsf). The depth interval assigned to an individual core begins with the depth below the seafloor at which core cutting began and extends to the depth where core cutting ended (see Fig. F1). The length of each cored interval

F1. Examples of numbered core sections, p. 39.
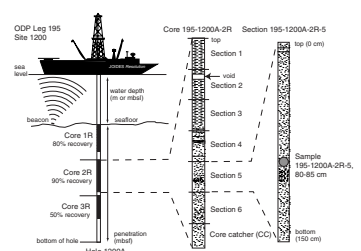
is generally 9.5 m, the length of a core barrel; however, coring intervals may be shorter and may not necessarily be continuous if separated by drilled intervals. In soft sediments, the drill string can be "washed ahead" with the core barrel in place without recovering sediments. This is achieved by pumping water down the pipe at high pressure to wash the sediment out of the way of the bit and up the space between the drill pipe and the wall of the hole.

Cores taken from a hole are numbered serially from the top of the hole downward. Core numbers and their associated cored intervals in meters below seafloor ideally are unique in a given hole; however, this may not be true if an interval is cored twice, if the borehole wall caves in, or other hole problems occur. Full recovery for a single core is 9.5 m of rock or sediment contained in a plastic liner (6.6 cm internal diameter) plus about 0.2 m (without a plastic liner) in the core catcher (Fig. F1). The core catcher is a device at the bottom of the core barrel that prevents the core from sliding out when the barrel is being retrieved from the hole. In many advanced hydraulic piston corer/extended core barrel (APC/XCB) cores, recovery exceeds the 9.5-m theoretical maximum by as much as 0.60 m. The cause of this expansion is at least partially a consequence of degassing. Each recovered core is divided while in its liner into 1.5-m sections that are numbered serially from the top (Fig. F1). When full recovery is obtained, the sections are numbered from 1 through 7, with the last section generally being shorter than 1.5 m. Rarely, a core may require more than seven sections; this is usually the result of gas expansion having caused voids within some sections. When less than full recovery is obtained, sections are numbered as needed to accommodate the length of the core; for example, 4 m of core would be divided into two 1.5-m sections and a 1-m section. If a core is fragmented (recovery <100%), the sections are numbered serially and remaining or unused sections are noted as void, whether shipboard scientists believe that the fragments were contiguous in situ or not. In rare cases, a section <1.5 m may be cut to preserve features of interest. Sections <1.5 m in length are also sometimes cut when the core liner is severely damaged.

By convention, material recovered from the core catcher is placed immediately below the last section when the core is described and is labeled core catcher (CC); in sedimentary cores, it is treated as a separate section. In cases where material is only recovered in the core catcher, it is assigned the depth of the top of the cored interval (this convention differs from that used in the early days of deep-sea drilling), although information from the driller or other sources may indicate from what depth it was actually recovered.

When the recovered core is shorter than the cored interval, the top of the core is equated with the top of the cored interval by convention to achieve consistency when handling analytical data derived from the cores. Samples removed from the cores are designated by distance, measured in centimeters from the top of the section to the top and bottom of each sample removed from that section. A complete identification number for a sample consists of the following information: leg, site, hole, core number, core type, section number, piece number (for hard rock), and interval in centimeters, measured from the top of section. For example, a sample identification of "195-1200A-7R-1, 10–12 cm" would be interpreted as representing a sample removed from the interval between 10 and 12 cm below the top of Section 1, Core 7 ("R" designates that this core was taken by the rotary core barrel) from Hole 1200A during Leg 195. A computer routine is available to calculate the

meters below seafloor depth from any correctly formulated ODP sample designation; this avoids inconsistencies that could have arisen on those occasions where some sections were cut to nonstandard lengths. Although meters below seafloor depth is an invaluable convention, it is not ideal, especially for high-resolution work.

All ODP core and sample identifiers indicate core type. The following abbreviations are used:

H = hydraulic piston core (HPC; also referred to as APC).
X = extended core barrel.
R = rotary core barrel (RCB).
W = wash core recovery.
G = ghost core.
M = miscellaneous material.

APC, XCB, RCB, G, and W cores were cut during Leg 195.

Core Handling

Sediments

As soon as a core is retrieved on deck, a sample is taken from the core catcher and taken to the paleontology laboratory for an initial age assessment. Then, the core is laid out on a long horizontal rack on the catwalk adjacent to the drilling floor. Next, the core is marked into section lengths, each section is labeled, and the core is cut into sections. Headspace gas samples are taken from the ends of cut sections on the catwalk and sealed in glass vials for light hydrocarbon analysis as part of the shipboard safety and pollution prevention program. During Leg 195, headspace gas samples of sediment were taken at both Sites 1200 and 1201. The plastic core liner containing each section is then sealed at the top and bottom by gluing on color-coded plastic caps: blue to identify the top of a section and clear to identify the bottom. Caps are usually attached to the liner by coating the end of the liner and the inside rim of the cap with acetone.

Next, the sections of core are carried into the laboratory and each is labeled again using an engraver to mark the full designation of the section permanently onto the plastic core liner. The length of the core in each section and the core catcher sample are measured to the nearest centimeter; this information is logged into the shipboard Janus database program. At this point, whole-round samples are taken for pore water and microbiology studies. After the remaining cores have equilibrated to room temperature (~3 hr), they are run through the multisensor track (MST), thermal conductivity measurements are performed on relatively soft sediments, and the cores are split.

Cores are split lengthwise into working and archive halves. The softer cores are split with a wire or saw, depending on the degree of induration. Harder cores are split with a band saw or diamond saw. During Leg 195, the wire-cut cores were split from the bottom to the top; thus, investigators should be aware that in the sediments material may have been transported up the core on the split face of each section.

The working half of the core is sampled for both shipboard and shore-based laboratory studies. Each extracted sample is logged into the sampling computer database program by the location and the name of the investigator receiving the sample. Records of all removed samples are kept by the curator at ODP. The extracted samples are sealed in plas-

tic vials or bags and labeled. Samples are routinely taken for shipboard physical properties and paleomagnetic measurements and for calcium carbonate (coulometric) analysis.

The archive half is described visually. Smear slides are made from sediment samples taken from the archive half. Most archive sections are run through the cryogenic magnetometer. The archive half is then photographed using both black-and-white and color film, a whole core at a time. Close-up photographs (color and black and white) are taken of particular features for illustrations in the summary chapter for each site, as requested by individual scientists.

Both halves of the core are then placed into labeled plastic tubes, sealed, and transferred to cold-storage space aboard the drilling vessel. At the end of the leg, the cores are transferred from the ship in refrigerated airfreight containers to cold storage at the Gulf Coast Repository of the Ocean Drilling Program at Texas A&M University.

Igneous, Metamorphic, and Ultramafic Rocks

Hard rock cores are handled differently from sedimentary cores. Once on deck, the core catcher sample is placed at the bottom of the core liner and total core recovery is calculated by shunting the rock pieces together and measuring the total length to the nearest centimeter. This information is logged into the shipboard Janus database program. The core is then cut into 1.5-m-long sections and transferred into the laboratory.

The contents of each section are transferred into 1.5-m-long sections of split core liner, where the bottom of oriented pieces (i.e., pieces that clearly could not have rotated top to bottom about a horizontal axis in the liner) are marked with a red wax pencil to ensure that orientation is not lost during splitting and labeling. Important primary features of the cores also are recorded at this time. The core is then split into archive and working halves. A plastic spacer is used to separate individual pieces and/or reconstructed groups of pieces in the core liner. These spacers may represent a substantial interval of no recovery. Each piece is numbered sequentially from the top of each section, beginning with number 1; reconstructed pieces are all assigned the same number but with a consecutive suffix letter (e.g., Piece 1A, 1B, etc.). Pieces are labeled only on the outer cylindrical surfaces of the core. If the piece is oriented, an arrow is added to the label pointing to the top of the section.

In splitting the core, every effort is made to ensure that important features are represented in both halves. The archive half is described visually and then photographed with both black-and-white and color film, one core at a time. Nondestructive physical properties measurements, such as magnetic susceptibility, are performed on the archive half of the core. The working half is sampled for shipboard physical properties measurements, paleomagnetic studies, inductively coupled plasma–atomic emission spectroscopy (ICP-AES), X-ray diffraction (XRD), and thin section studies. The working half of the hard rock core then is sampled for shore-based laboratory studies. Records of all samples are kept by the curator at ODP. Both halves of the core are then shrink-wrapped in plastic to prevent rock pieces from vibrating out of sequence during transit, placed into labeled plastic tubes, sealed, and transferred to cold-storage space aboard the drilling vessel. As with the other Leg 195 cores, they are housed at the Gulf Coast Repository of the Ocean Drilling Program at Texas A&M University.

LITHOSTRATIGRAPHY

This section outlines procedures to document the basic sedimentology of the deposits recovered during Leg 195, including lithologic classification, core description, smear slide description, color spectrophotometry, and X-ray diffraction.

Lithologic Classification

The description of Leg 195 lithologies follows the ODP classification scheme (Mazullo et al., 1988). Composition of biogenic components and texture of siliciclastic particles are the definition criteria for sedimentary lithologies. Biogenic components consist of the skeletal remains of open-marine calcareous and siliceous microfauna and microflora derived from foraminifers, coccolithophorids (nannofossils), and radiolarians, as well as subordinate diatoms, sponge spicules, and silicoflagellates. Siliciclastic detrital components are composed of quartz, feldspar, heavy minerals, and clay minerals, as well as lithic rock fragments. Moreover, volcaniclastic components are intercalated in sediment sequences. At Site 1200, where we drilled into the summit of a mud volcano, serpentine deposits comprise the principal lithology. The principal name of a lithology refers to the component that exceeds 50% of the total composition.

Biogenic Sediments

The principal name of biogenic sediments and sedimentary rocks relates to the chemical composition, the major components, and the degree of compaction and induration. The following names are used: "ooze" for unconsolidated calcareous and/or siliceous biogenic sediments, "chalk" for friable biogenic sediment composed predominantly of calcareous biogenic grains, and "chert" for indurated biogenic sediment composed predominantly of siliceous biogenic grains.

The principal name of the biogenic sediment is preceded by major modifiers and followed by minor modifiers that may refer to mixed biogenic oozes and siliciclastic components. Sediments containing >50% siliciclastic material are classified separately (see "Siliciclastic Sediments," p. 6). Components in the range of 25%–50% modify the principal name (e.g., foraminifer ooze, nannofossil chalk, and radiolarian chert). In some cases, the identification and differentiation of individual components could be ambiguous, so we relate to more informal terms such as calcareous ooze or biosiliceous ooze. Components in the range of 10%–24% are added with the suffix "-bearing" (e.g., foraminifer-bearing nannofossil ooze). Components with abundances <10% are not named unless they are very important for interpretation (e.g., foraminifer-bearing radiolarian ooze with minor diatoms).

Biogenic sediments including between 25% and 50% siliciclastics are not referred to as oozes, chalks, or cherts. In this case, the principal name is followed by textural assignment of the major siliciclastic grain size (e.g., foraminifer silt or diatom-bearing nannofossil clay).

Siliciclastic Sediments

Siliciclastic sediments are composed of detrital mineral and rock fragments derived from plutonic, sedimentary, and metamorphic rocks. If the total siliciclastic component of the sediment is >50%, the principal

name is determined by the relative proportions of sand, silt, and clay grain sizes when plotted on a Shepard (1954) classification diagram (Fig. F2). For siliciclastic sediments, the principal name describes the texture and is assigned according to the following guidelines:

1. The Udden-Wentworth grain-size scale (Wentworth, 1922), which defines the grain-size ranges and the names of the textural groups (gravel, sand, silt, or clay) that are used as the principal names of siliciclastic sediments.
2. When two or more textural groups are present in a siliciclastic sediment in sufficient amounts, principal names are listed in order of increasing abundance.
3. The suffix "-stone" is affixed to the principal name sand, silt, or clay when the sediment is lithified (e.g., sandstone).

Debris-flow facies encountered at Site 1200 (South Chamorro Seamount) are characterized by poorly sorted serpentine diamict facies. The term diamict is used as a nongenetic term for materials consisting of matrix-supported admixtures of clasts (defined here as fragments larger than sand size [2 mm]). It should be noted that existing ODP classifications do not adequately address nonsorted or poorly sorted admixtures of siliciclastic sediments, such as diamicts. The classification of poorly sorted sediments containing gravel is based on Moncrieff (1989) (Fig. F3). Clast-supported admixtures are named conglomerates when the clasts are rounded and breccia when the clasts are angular.

The following two classes of induration or lithification for siliciclastic sediments were adopted and modified from Leg 105 (Shipboard Scientific Party, 1987):

1. Soft: diamicton, sand, silt, clay (sediment core can be split with a wire cutter); and
2. Hard: diamictite, sandstone, siltstone, claystone (cannot be compressed with finger pressure, or core must be cut with a band saw or diamond saw).
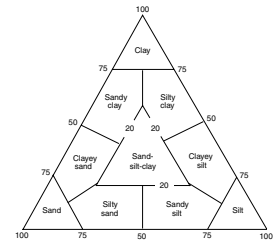
Volcaniclastic Deposits

Although the sedimentary succession at Site 1201 in the Philippine Basin contains abundant detrital volcaniclastic material, the deposits are not referred to as primary volcaniclastic sediments because they were subsequently reworked and redeposited by turbidity currents. As a result, they have been classified as siliciclastic sediments (see "Siliciclastic Sediments," p. 6).

Serpentine Deposits

Like volcaniclastic rocks, serpentine deposits represent lithologies that cannot clearly be related to one genetic mode. Although they originate from disaggregated metamorphosed ultramafic rocks, their emplacement via cold gravitational flows implies sedimentary processes. Here, we adopt the classification scheme of serpentine deposits developed by Leg 125 scientists (Shipboard Scientific Party, 1990). This classification includes the degree of compaction, mineralogical composition, and structural features. Serpentine deposits contain >50% serpentine-rich material in association with other primary or secondary authigenic minerals, such as aragonite, chlorite, epidote, and zoisite. Unconsoli-

F2. Textural classification scheme for siliciclastics, p. 40.

F3. Classification of poorly sorted sediments with a gravel component, p. 41.

dated material is referred to as serpentine and indurated material as serpentinite, respectively. When serpentine is present in amounts <50% or is not associated with nonbiogenic aragonite >50%, the sediment and sedimentary rock classification scheme previously described is used.

The principal name of serpentine deposits is preceded by appropriate textural and compositional modifiers. The textural modifier is placed nearest the principal name and defines the dominant grain size (e.g. silt-sized serpentine or sand-sized serpentine). The compositional modifiers are listed in order of decreasing abundance to the left of the textural modifier and the principal name. Here, our classification differs slightly from that of Leg 125 so that our use of modifiers is consistent with nomenclature techniques used in previous sections of this chapter. A value of 25%–50% of a component qualifies for major compositional modifier status (e.g., chlorite sand-sized serpentine). A value of 10%–24% of a component qualifies for minor compositional modifier status and is hyphenated with the word "-bearing." (e.g., zoisite-bearing sand-sized serpentine). A value of <10% of an unusual important component (e.g., aragonite) qualifies for minor compositional modifier status (e.g., zoisite-bearing, chlorite silt-sized serpentine with minor aragonite).

Serpentinites are frequently brecciated. If large clasts are set in a finer-grained serpentine matrix, then the material is named serpentinite breccia (without tectonic or sedimentary implications) with subsequent modifiers describing the matrix. Sheared phacoidal serpentine is composed of scales or chips of serpentine ≥1 mm in size, which may have slickensided surfaces and whose long axes define an anastomosing foliation. This foliation may enclose angular to subangular blocks of unsheared serpentinite (≥1 cm in size) or may be associated with horizontal or vertical convolute bedding.
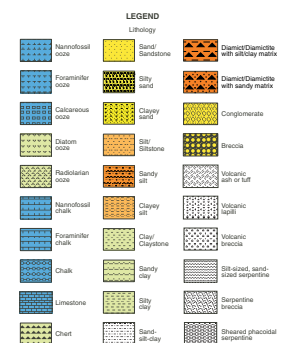
Visual Core Description

Information from the macroscopic description of each core was recorded manually for each core section on visual core description forms (VCDs). This information was condensed and entered into AppleCORE (version 8.1b) software, which generates a simplified, one-page graphical description of each core ("barrel sheet"). Barrel sheets are presented with split-core photographs (see the "Core Descriptions" contents list). The lithologies of the recovered sediments are represented on barrel sheets by symbols in the column entitled "Graphic Lithology" (Fig. F4).

The color (hue and chroma) of the sediments was determined visually using the Munsell soil color charts (1975). A wide variety of features that characterize the sediment, such as bed thicknesses, primary sedimentary structures, bioturbation parameters, soft-sediment deformation, and structural and diagenetic features are indicated in columns to the right of the graphic log. The symbols are schematic but are placed as close as possible to their proper stratigraphic position. (For exact positions of sedimentary features, the detailed section-by-section paper core description forms produced on the ship can be obtained from ODP.)

Bed thickness is characterized by the terms "very thick bedded" (>100 cm thick), "thick bedded" (30–100 cm thick), "medium bedded" (10–30 cm thick), "thin bedded" (3–10 cm thick), and "very thin bedded" (1–3 cm thick) (McKee and Weir, 1953). Stratigraphic intervals <1 cm thick are characterized by the term "lamination."

Deformation and disturbance of sediment that resulted from the coring process are indicated by symbols in the "Drilling Disturbance" col-

umn (Fig. F4). Blank regions indicate the absence of coring disturbance. Detailed accounts of drilling disturbance appear in many previous ODP reports (e.g., Shipboard Scientific Party, 1995). Locations of samples taken for shipboard analysis are indicated in the "Samples" column.

A summary lithologic description with sedimentologic highlights is given in the "Remarks" column of the barrel sheet. This description provides information about the major sediment lithologies, important minor lithologies, an extended summary description of the sediments, including color, composition, sedimentary structures, trace fossils identified, extent of bioturbation, the age of the sediments as determined by shipboard paleontologists and paleomagnetists, and other notable characteristics. Descriptions and locations of thin, interbedded, or minor lithologies that could not be depicted in the "Graphic Lithology" column are presented in "Remarks," where space permits.

Smear Slides and Thin Sections

Lithologic characterization on the basis of visual core descriptions was verified by analyses of smear slides and thin sections, which provide crude estimates of grain-size distributions and the relative abundances of biogenic, siliciclastic, volcanic, and serpentine constituents. The visual estimates are based on area proportions and are qualitative in nature. Fine-grained particles such as clays and nannofossils are often underestimated. At Site 1201, the thin sections also provide insights into the diagenetic features of sandstones. The positions of smear slide and thin section samples taken from each core for shipboard analysis are indicated by "SS" and "TS" in the "Sample" column on the core description form.

Spectrophotometer

Reflectance of visible light from the surface of cores was routinely measured downcore using a Minolta spectrophotometer (model CM-2002) mounted on the archive multisensor track (AMST). The AMST measures the archive half of each core section. The purpose of measuring the visible light spectra was to provide a continuous stratigraphic record of color variations downcore for visible wavelengths (400–700 nm). Spectrophotometer readings were taken when the core sections were wet and after the surface of each core section was cleaned. The measurements were then automatically taken and recorded by the AMST, which permits measurements at evenly spaced intervals along each core. Each measurement consists of 31 separate determinations of reflectance in 10-nm-wide spectral bands from 400 to 700 nm. Additional detailed information about the measurement and interpretation of spectral data with the Minolta spectrophotometer can be found in Balsam et al. (1997, 1998, 1999, 2000).

X-Ray Diffraction

Relative abundances of the main silicate and carbonate minerals were determined semiquantitatively on both the bulk sediment fraction (Sites 1200 and 1201) and on the clay fraction (Site 1201) using a Philips model PW1729 X-ray diffractometer with CuK_α radiation (Ni filter).

Each bulk sediment sample was freeze-dried, crushed, and mounted with a random orientation in an aluminum sample holder. Instrument conditions were as follows: 40 kV, 35 mA, goniometer scan from 2° to

70°2θ for bulk samples, step size = 0.01°2θ, scan speed = 1.2°2θ/min, and count time = 0.5 s. Peak intensities were converted to values appropriate for a fixed slit width. An interactive software package (MacDiff 4.0.4 PPC) was used on a Macintosh computer to identify the primary minerals (public domain software is available on the World Wide Web from http://www.pangaea.de). Diffractograms were peak-corrected to match the primary quartz peak at 3.343 Å. In the absence of quartz, no peak correction was applied. Identifications are based on multiple peak matches, using the mineral database provided with MacDiff. Relative proportions of quartz, feldspar, carbonates, serpentine, brucite, zeolites, carbonates, and clay minerals were estimated using peak intensity ratios. Relative abundances reported in this volume are useful for general characterization of the sediments but are not precise quantitative data.

Clay mineralogy was also examined and verified by XRD on selected subsamples of the clay fraction (≤2 μm). For grain-size separation, 3-g samples of bulk sediment were disaggregated and washed with 25 mL of distilled water in 50-mL centrifuge tubes. Centrifuging for 15 min at 1500 rounds per minute (rpm) removed salt from the samples. After decanting the wash water, 25 mL of Calgon solution was added to the samples in 50-mL beakers. The samples were then placed in a sonic bath for up to 15 min to suspend the clays by ultrasonic disaggregation and then centrifuged for 5 min at 1000 rpm to settle the >2-μm particles. The clays that remained in suspension were collected from the top 1 cm of the solution with an eye dropper. Two oriented clay mounts of each sample were made by placing drops of the clay solution onto glass slides that were then dried at room temperature. One slide was first analyzed in the air-dried state. Then it was solvated with ethylene glycol for at least 12 hr and reanalyzed to determine the presence of expandable clays. The second slide was analyzed after being heated to 550°C for 1 hr to collapse kaolinite and smectite. All oriented clay mounts were scanned from 2° to 35°2θ in 0.010° increments.

IGNEOUS PETROLOGY

The recovered core from Site 1200 consists of clasts of variably metamorphosed ultramafic rocks included in unconsolidated fine-grained serpentine muds. The muds that comprise the matrix of this cored material were, however, not formed by sedimentary processes. They consist of finely comminuted rock and mineral fragments and secondary products derived from the serpentinization of ultramafic rocks and metamorphism of mafic rocks. Although such fine-grained materials were described as sediments during Leg 125 (Shipboard Scientific Party, 1990), they were, in fact, igneous and metamorphic rocks. For consistency with ODP format, the descriptions of the serpentine mud were noted on barrel sheets for sedimentary material and the petrologists and sedimentologists worked together to finalize the description of the material. The clasts of serpentinized ultramafic rocks recovered from Site 1200 and the basement material recovered from Site 1201 were described on the hard rock visual core description sheets using standard ODP igneous petrology procedures.

General Procedures

The general procedures used during Leg 195 for describing igneous rocks from Sites 1200 and 1201 follow the outline presented in the "Explanatory Notes" chapters of Legs 125 and 176 (Shipboard Scientific Party, 1990, 1999, respectively). All qualitative and quantitative measurements (e.g., grain size, percent alteration, etc.) were made by consensus. Visual igneous, metamorphic, and structural characteristics were included in the documentation of each core to better describe important characteristics, such as alteration style, mineralogy, and the occurrence of veins. Identification of mineral phases was checked by XRD analyses according to ODP standard procedures outlined in previous *Initial Reports* volumes (e.g., Leg 118; Shipboard Scientific Party, 1989). At least one minicore was taken per lithologic unit for chemical and physical properties analyses, generally from the freshest part of the core. Additional thin sections, XRD, and ICP-AES analyses were performed on selected samples of specific interest (vein material, highly or less-altered intervals, and coarse-grained intervals).

Macroscopic Descriptions

Igneous VCD forms were used when describing the basement cores (Fig. F5). Where possible, the primary and secondary phases in hand specimen were noted. The volume content of the phases present was estimated and verified by examination of representative thin sections. Colors of the recovered material were determined using Munsell soil color charts on dry, cut faces of cores.

Thin Section Descriptions

Thin section billets of igneous and metamorphic rocks were examined (1) to confirm the identity of petrographic groups in the cores, (2) to better understand the textures and interrelationships of the mineral phases, (3) to help define unit boundaries indicated by hand specimen core descriptions, and (4) to define the secondary alteration mineralogy. Percentages of individual mineral phases were visually estimated and reported on thin section description sheets. Wherever possible, approximate composition of preserved primary minerals has been determined by means of their optical properties.

Primary (olivine, orhopyroxene, clinopyroxene, spinels, feldspars, and amphibole) and secondary (serpentine, chlorite, brucite, iron oxide and hydroxide, carbonate, clay minerals, zeolites, apatite, talc, and mica) phases were identified in thin sections. Each of the minerals were recorded on thin section description forms (Fig F6). The information includes the following major observations:

1. Modal percent estimate;
2. Smallest, largest, and average sizes of mineral grains (measured along the longest axis, in millimeters);
3. Average grain size of the rock: fine grained (<1 mm), medium grained (1–5 mm), and coarse grained (>5 mm);
4. Mineral shape, using terms such as fibrous, prismatic, bladed/lath shaped, lamellar, tabular/platy, equant, etc.;
5. Mineral habit, using the terms euhedral, subhedral, anhedral, dendritic, and skeletal;

F5. Descriptive names for coherent lavas and intrusions, p. 44.

F6. Spreadsheet for thin section description, p. 45.

6. Groundmass texture: bastitic, hourglass, and mesh applied to serpentinized ultramafic rocks from Site 1200; glassy (contains volcanic glass only), felty, intersertal, intergranular, hyalopilitic, ophitic, subophitic, spherulitic, and branching applied to basement rocks from Site 1201;

7. Vesicles: percentage abundance, distribution, size, shape, and fillings and their relationships (including proportion of vesicles that are filled by alteration minerals, namely amygdules); and

8. Mineral occurrence, if minerals occurred as chadacrysts or oiko-crysts, meaning that one crystal completely encloses another smaller crystal, where oikocrysts are the enclosing crystal and chadacrysts are the enclosed crystals.

Basalts are termed aphyric (<1%), sparsely phyric (1%–2%), moderately phyric (2%–10%), or highly phyric (>10%), depending upon the proportion of phenocrysts visible with a hand lens or binocular microscope (~10× magnification). Basalts were further classified by phenocryst type (e.g., a moderately plagioclase-olivine phyric basalt contains 2%–10% phenocrysts, mostly plagioclase, with subordinate olivine).

Serpentinized rocks were classified on the basis of the original phase proportions present in the protolith, using the International Union of Geological Societies classification system for ultramafic rocks. For example, "serpentinized dunite" is a rock with at least 90% modal olivine originally present.

Alteration was addressed through XRD analyses and studies of the occurrence of secondary minerals in thin sections. The XRD analyses were able to distinguish mineral groups and varieties, such as serpentines, clays, chlorite group minerals, and secondary iron oxide minerals. From thin section analyses, it was possible to identify vein-filling materials (serpentine varieties, carbonates, chlorite, and talc) and pseudomorphic textures (serpentine and brucite after olivine; serpentine and talc after orthopyroxene in serpentinized ultramafic rocks from Site 1200; clay minerals, chlorite, iron oxides and hydroxides, and carbonate after olivine; and zeolites, chlorite, and alkali feldspar after plagioclase in basement rocks from Site 1201).

Rock Classification

Igneous rocks were classified based on their principal mineralogy. Ultramafic and mafic rock varieties were named according to the Streckeisen (1974) classification diagram based on olivine, clinopyroxene, orthopyroxene, and plagioclase abundances (Fig. F7). The volcanic rock samples were classified according to standard petrographic techniques, using a combination of modal mineralogy determinations and composition data from onboard ICP-AES analyses. The classical double triangle Streckeisen (1974) classification diagram was also used (Fig. F8).

ICP-AES Analysis

We selected representative samples of major lithologic units for shipboard ICP-AES analysis. Large whole-rock pieces were first cut with a diamond-impregnated saw and ground on a diamond wheel to remove surface contamination. Samples were washed in an ultrasonic bath containing methanol for ~10 min. This was followed by three consecutive ~10-min washes in an ultrasonic bath containing nanopure deionized water, then the samples were dried for ~12 hr in an oven at 110°C. The

F7. Classification diagram for mafic and ultramafic rock, p. 46.

F8. Streckeisen classification diagram for volcanic rocks, p. 47.

cleaned whole-rock samples (~15 cm³) were reduced to fragments <1 cm in diameter by crushing between two disks of Delrin plastic in a hydraulic press and ground for ~5 min in a Spex 8510 shatterbox with a tungsten carbide barrel. The sample powders were weighed on a Scientech balance and ignited to determine the weight after loss on ignition.

We weighed 0.100 ± 0.002-g aliquots of the ignited whole-rock powders and mixed them with 0.4000 ± 0.0004 g of lithium metaborate ($LiBO_2$) flux that had been preweighed on shore. Standard rock powders and full procedural blanks were included with the unknowns for each sample run. All samples and standards were weighed on the Scientech balance. Weighing errors were conservatively estimated to be ±0.0005 g.

Mixtures of flux and rock powders were fused in Pt-Au crucibles at 1050°C for 10–12 min in a bead sampler NT-2100. Ten microliters of 0.172-mM aqueous lithium bromide (LiBr) solution was added to the mixture before fusion as an antiwetting agent to prevent the cooled bead from sticking to the crucible. Cooled beads were transferred to 125-mL polypropylene bottles and dissolved in 50 mL of 2.3-M HNO_3 by shaking with a Burrell wrist-action bottle shaker for 1 hr. After digestion of the glass bead, all of the solution was passed through a 0.45-µm filter into a clean 60-mL wide-mouth polypropylene bottle. Next, 2.5 mL of this solution was transferred to a plastic vial and diluted with 17.5 mL of 2.3-M HNO_3 to bring the total volume to 20 mL. The solution-to-sample dilution factor for this procedure is 4000.

Major (Si, Ti, Al, Fe, Mn, Mg, Ca, Na, K, and P) and trace (Zr, Y, Sr, Ba, Zn, Cu, V, Cr, and Ni) element concentrations of powder samples were determined with the JY2000 Ultrace ICP-AES. The JY2000 sequentially measures characteristic emission intensities (with wavelengths between ~100 and 800 nm). ICP-AES protocols for dissolution and analysis of rock powders were developed by Murray et al. (2000). The elements analyzed, their units, and the ICP-AES detection limits for Leg 195 samples are provided in Table T1.

A typical ICP-AES run includes

1. A set of certified rock standards (PCC-1, JP-1, BIR-1, JGB-1, W-2, BHVO-2, G-2, and AGV-1) run at the beginning, middle, and end of the sample run;
2. A set of unknown samples;
3. A drift-correcting reference standard (K-1919) analyzed every fourth sample position; and
4. A blank solution run near the beginning, middle, and end of each run.

A 2.3-M HNO_3 wash solution was run for a minimum of 90 s between each of the samples and standards.

Following each sample run, the raw intensities were transferred to a data file and data reduction was completed using a spreadsheet to ensure proper control over standardization and drift correction. Once transferred, intensities for all samples were corrected for the full procedural blank. Drift correction was then accomplished by linear interpolation between each consecutively run drift-correcting solution and correcting the intensities of the samples run between those drift-correcting solutions. The interpolation was calculated using the lever rule. Following blank subtraction and drift correction, concentrations for each sample were calculated from the average intensity per unit concentration for the rerun certified reference material.

Estimates of accuracy and precision for major and trace element analyses were based on replicate analyses. In general, run-to-run relative precision by ICP-AES was ~2% for the major elements. Run-to-run relative precision for trace elements was generally ~5%–10%. Exceptions typically occurred when the element in question was near the detection limit of the instrument (Table T1).

BIOSTRATIGRAPHY

During Leg 195, calcareous nannofossils were studied to assess biostratigraphic constraints on the sedimentary sections at Sites 1200, 1201, and 1202. Ages for calcareous nannofossil events in the Paleogene and Miocene were determined according to the geomagnetic polarity timescale of Cande and Kent (1995), with minor modification for the Pliocene and Pleistocene using the astrochronology of Lourens et al. (1996). Astronomically tuned datum levels were used whenever possible. Foraminifers in the nannofossil-bearing serpentine mud intervals of Site 1200 were also examined to assist in interpreting the depositional environment and the taphonomy of the microfossils.

Calcareous Nannofossils

We have referred primarily to the zonations of Martini and Müller (1986) for Cenozoic sediments. Numerical ages used are those compiled by Berggren et al. (1995b) (Fig. F9) to facilitate easy comparison with other studies. Calcareous nannofossil assemblages were described from smear slides prepared for each core catcher sample and for as many additional core samples as time permitted. Standard smear slides were made for all samples using Norland optical adhesive as a mounting medium. Examination was performed exclusively with a light microscope, using whatever optical configuration yielded useful results. Unless otherwise noted, we followed taxonomic concepts summarized in Perch-Nielsen (1985). In all cases, a magnification of 1000× was used to make semiquantitative estimates of abundances of individual species. Five levels of abundance were recorded, with the following approximate definitions:

R = rare (1 specimen per 51 or more fields of view).
F = few (1 specimen per 11–50 fields of view).
C = common (1 specimen per 2–10 fields of view).
A = abundant (1–10 specimens per field of view).
V = very abundant (>10 specimens per field of view).

The total abundance of calcareous nannofossils for each sample was estimated as follows:

B = barren (none).
R = rare (1–10 specimens for 500 fields of view [about three traverses]).
F = few (11–50 specimens for 500 fields of view).
C = common (51–2,000 specimens for 500 fields of view).
A = abundant (2,001–20,000 specimens for 500 fields of view).
V = very abundant (>20,000 specimens for 500 fields of view).

F9. Nannofossil datums, p. 48.
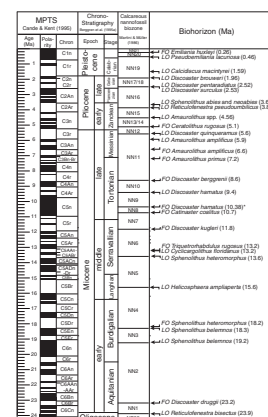
The qualitative evaluation of the preservation of calcareous nannofossils was recorded as poor (P), moderate (M), good (G), or very good (VG), as prescribed in the Janus database system. These categories represent subjective impressions according to the following definitions:

P = poor. Severe dissolution, fragmentation, and/or overgrowth has occurred. Primary features may have been destroyed, and many specimens cannot be identified at the species level.

M = moderate. Dissolution and/or overgrowth is evident. A significant proportion (up to 10%) of the specimens cannot be identified to species level with absolute certainty.

G = good. There is little or no evidence of dissolution and/or overgrowth. Diagnostic characteristics are preserved, and nearly all specimens can be identified to species level.

VG = very good. No evidence of dissolution and or secondary overgrowth; diagnostic characteristics are perfectly preserved.

Foraminifers

Core catcher samples of ~20 cm³ or more were washed in tap water over a 150-µm mesh sieve to retrieve free microfossil specimens. Washed residues were dried in an oven at ~50°C. The dried samples were examined under a binocular microscope, and the foraminifer faunal composition was recorded in qualitative terms, based on an assessment of species observed in a random sample from the >150-µm size fraction. Relative abundances were reported using the following categories:

A = abundant (>30%).
C = common (16%–30%).
F = few (4%–15%).
R = rare (2%–3%).
T = trace (<2%).

Preservation of planktonic foraminifer assemblages was recorded as follows:

G = good (little or no evidence of dissolution or recrystallization/replacement).

M = moderate (moderate signs of dissolution or recrystallization/replacement; nearly all specimens can be identified at the species level).

P = poor (severe signs of dissolution or recrystallization/replacement; primary features are largely destroyed).

PALEOMAGNETISM

Paleomagnetic studies conducted on board the *JOIDES Resolution* during Leg 195 consist of remanent magnetization measurements of archive-half sections before and after alternating-field (AF) demagnetization, magnetic remanence measurements on discrete samples collected from the working half of core sections, magnetic susceptibility measurements on whole-core sections, and a limited set of rock-magnetic measurements on discrete samples. Discrete samples were collected from

working halves in standard 8-cm³ plastic cubes with the arrow on the bottom of the sampling box pointing upcore. Hard rock samples were either cut using a parallel saw or drilled using a nonmagnetic drill. The sampling frequency for rock-magnetic characterization was one sample per core at Site 1200 and one to two samples per core section at Site 1201. Sampling at Site 1202 was restricted to six oriented discrete samples because of time constraints at the end of Leg 195. Intervals of drilling-related core deformation were avoided.

Instruments and Measurement Procedure

Measurements of remanent magnetization were carried out using an automated pass-through cryogenic direct current superconducting quantum interference device (DC-SQUID) magnetometer (2-G Enterprises model 760-R) with an in-line AF demagnetizer (2-G Enterprises model 2G600) capable of producing peak fields of 80 mT with a 200-Hz frequency. The background noise level of the magnetometer onboard environment is ~3×10^{-10} Am². The large volume of core material within the sensing region of the magnetometer, which is on the order of 100 cm³, permits accurate measurements of cores with remanent intensities as weak as ~10^{-5} A/m.

The standard ODP magnetic coordinate system was used (+x: vertical upward from the split surface of archive halves; +y: left along split surface when looking upcore; and +z: downcore).

Natural remanent magnetization was routinely measured for all sedimentary archive-half sections at 5-cm intervals. Measurements at core and section ends and within intervals of drilling-related core deformation were edited during data processing. AF demagnetization was applied at 5, 10, 15, and 20 mT. All discrete sample measurements were also made on the pass-through magnetometer using a sample boat that held six discrete cube samples at 20-cm intervals.

Discrete samples were AF demagnetized using the in-line demagnetizer installed on the pass-through cryogenic magnetometer at 5-mT steps to 40 mT and at 10-mT steps to 80 mT. An Analytical Services Company model IM-10 impulse magnetizer, which can apply pulsed fields from 20 to 1200 mT, was used for studies of the acquisition of stepwise isothermal remanent magnetization (IRM), saturation IRM (SIRM), and backfield SIRM of selected discrete samples. The SIRM of selected discrete samples was thermally demagnetized using a Schonstedt model TSD-1 thermal specimen demagnetizer at 100° steps to 300°C, 50° steps to 550°C, and 20° steps to 640°C. Spurious fields inside the oven do not exceed 100 nT and are generally <5 nT inside the cooling chamber. Temperature gradients over the central 30.5-cm length of the oven are on the order of 10°C, with an absolute temperature accuracy within 20°C of the set value. An anhysteretic remanent magnetization was imparted to each discrete sample by exposing it to both a constant 0.05-mT field and a slowly decaying 100-mT alternating field. The low-field volume susceptibility for discrete samples was measured using a Bartington MS2 meter attached to a MS2C sensor with a coil diameter of 33 mm.

Magnetic susceptibility was measured for each whole-core section as part of the MST analysis (see **"Physical Properties,"** p. 19). The MST susceptibility meter (a Bartington MS2 meter containing an MS2C sensor with a coil diameter of 88 mm and an inducing field frequency of 0.565 kHz) was set on SI units, and the values were stored in the Janus database in raw meter units. To convert to true SI volume susceptibili-

ties, these values were multiplied by 10^{-5} and then multiplied by a correction factor to take into account the volume of material that passed through the susceptibility coils. The correction factor for a standard ODP core is ~0.66 (= 1/1.5). This correction was applied for all figures illustrating magnetic susceptibilities in the "Paleomagnetism" sections in each site chapter of this volume. The data were not corrected for undersized core, core gaps, or the end effects of each section.

Core Orientation

Core orientation of the APC was achieved with a Tensor tool mounted on the core barrel. The Tensor tool consists of a three-component fluxgate magnetometer and a three-component accelerometer rigidly attached to the core barrel. The information from both sets of sensors allows the azimuth and dip of the hole to be measured, as well as the azimuth of the double-line orientation mark on the core liner. Orientation is not usually attempted for the top three cores (~30 mbsf) until the bottom-hole assembly is sufficiently stabilized in the sediment. Core orientation by the Tensor tool is relative to magnetic north.

Magnetostratigraphy

Where AF demagnetization successfully isolated the primary component of remanent magnetization, paleomagnetic inclinations and declinations were used to assign a magnetic polarity to the stratigraphic column. An interpretation of the magnetic polarity stratigraphy, with constraints from the biostratigraphic data, is presented in the "Site 1201" chapter. The magnetic polarity timescale of Cande and Kent (1995) and timescale of Berggren et al. (1995b) were used.

GEOCHEMISTRY

Sediment Geochemistry

Sediments were analyzed for inorganic carbon and for total hydrogen, nitrogen, carbon, and sulfur. The organic carbon content of the sediments was then calculated by difference. All samples were freeze-dried prior to analysis.

Total inorganic carbon was determined using a Coulometric 5011 coulometer equipped with a System 140 carbonate carbon analyzer. Depending on carbonate content, 15–20 mg of ground and weighed sediment was reacted in a 2-N HCl solution. The liberated CO_2 was titrated in a monoethanolamine solution with a colorimetric indicator while monitoring the change in light transmittance with a photodetection cell.

Total hydrogen, nitrogen, carbon, and sulfur were determined using an H/N/C/S analyzer, model NA 1500 from Carlo Erba Instruments. Bulk samples were combusted at 1000°C in an oxygen atmosphere, converting organic and inorganic carbon to CO_2 and sulfur to SO_2. These gases, along with nitrogen, were then separated by gas chromatography and measured using a thermal conductivity detector.

Fluid Geochemistry

Hydrocarbon Gases

As required for safety considerations, the concentrations of the hydrocarbons methane (C_1), ethane (C_2), and propane (C_3) were monitored in the sediment cores. Hydrocarbon gases were extracted from bulk sediment using a headspace sampling technique. As soon as the core arrived on deck, a 5-cm^3 plug of sediment was taken using a number four cork borer. This sample was placed immediately in a glass vial that was then sealed with a septum and metal crimp seal and heated to 70°C. The gas driven off was drawn into a glass gas-tight syringe and injected into a Hewlett Packard 6890 series gas chromatograph equipped with a flame ionization detector. Where high concentrations of propane were suspected, a second sample was taken by the same method and analyzed for C_1 through C_6 hydrocarbons using a Hewlett Packard 6890 series natural gas analyzer, a gas chromatograph equipped with Poropak-Q, molecular-sieve, and silicone-oil coated columns and both flame ionization and thermal conductivity detectors. After the headspace gas was analyzed, the actual volume of the sediment sample was measured to the nearest 0.5 cm^3 by water displacement.

Samples of suspected gas pockets in the cores were also analyzed using the Hewlett Packard natural gas analyzer. These samples were taken immediately upon recovery of the core by penetrating the transparent plastic core liner with a hollow stainless steel punch equipped with a valve and hypodermic needle. The gases were injected directly into the gas chromatograph using a three-way nylon valve.

Interstitial Water

During Leg 195, interstitial water was obtained from sediments and unconsolidated serpentine by squeezing whole-round sections of core, 5–15 cm in length. As soon as the core arrived on deck, these samples were cut by slicing the polycarbonate core tube and capping both ends. The samples were then cooled from a typical arrival temperature of 15°–20°C to the appropriate in situ temperature, removed from the core liner, scraped with a stainless steel spatula to remove the outer contaminated layer, and placed in a titanium piston-cylinder squeezer (Manheim and Sayles, 1974). Both the squeezer and the samples were handled only with plastic gloves to avoid contamination. The squeezer was placed in a Carver hydraulic press and squeezed at pressures that were increased slowly up to 40,000 psi. Interstitial water was collected through an on-line 0.45-µm polysulfone filter mounted in a Gelman "acrodisc" disposable filter holder into a 50-mL plastic syringe, from which the various aliquots for analysis were ejected.

The water sampler temperature-pressure (WSTP) tool (Barnes, 1988) was used only once during Leg 195, to collect borehole water from Hole 1200C when it was suspected that formation fluid might be upwelling through the hole. (This was proved not to be the case, as the sample recovered was seawater.) The sampler is lowered on the sand line and locked into an assembly just above the bit so that the sampling probe projects ~20 cm through the bit. A timer-operated valve opens and draws water under negative pressure through a series of screens and filters into a 93-mL stainless steel coil and then into a 1.2-L steel overflow chamber that is initially filled with air and also contains the sample coils and valves. The coil is initially filled with distilled water that is dis-

placed by the sample. After sampling, the overflow chamber contains sampled water diluted by distilled water displaced from the coil. Water from both the sample coil (the WSTP-1 "prime" aliquot) and the overflow chamber (the WSTP-1 "overflow" aliquot) was analyzed.

The waters were analyzed immediately after recovery for pH, alkalinity (±1.5%) by potentiometric Gran titration, and hydrogen sulfide (±4%) by colorimetry using methylene blue.

Aliquots were refrigerated and analyzed within a few days of collection for chlorinity (±0.4%) and calcium (±0.7%) by electrochemical titration, magnesium (total alkaline earths; ±0.5%) by colorimetric titration, sulfate (±1%) and potassium (±2%) by ion chromatography (IC), ammonium (±4%) and phosphate (±4%) by colorimetry, fluoride by ion-specific electrode, and strontium, barium, manganese, iron, boron, aluminum, silicon, and lithium by ICP-AES. Sodium was calculated from charge balance. Chloride (±1%), sodium (±2%), calcium (±2%), and magnesium (±5%) were also determined by IC and the results used to check the accuracy of the more precise techniques noted above; for low concentrations (<3 mM) of calcium and magnesium where the titration results are inaccurate, the IC data were used instead. Except for the electrochemical end point detection used in the chlorinity and calcium titrations, all shipboard analyses were performed using standard ODP techniques, as detailed by Gieskes et al. (1991). International Association for the Physical Sciences of the Ocean standard seawater was the primary standard for determination of calcium, magnesium, potassium, sulfate, and chlorinity and also provided a check on the accuracy of the analyses for alkalinity and fluoride. Borax solutions were used as standards for the alkalinity titration.

PHYSICAL PROPERTIES

Shipboard measurements of physical properties provide quantitative information about the composition and lithology of core material and are used to characterize lithologic units and to correlate core data with downhole logging and seismic reflection data. All physical properties measurements were taken on cores after they equilibrated to room temperature (~25°C). Equilibration to room temperature takes 2–4 hr. Magnetic susceptibility, gamma ray attenuation bulk density, compressional wave (*P*-wave) velocity, and natural gamma radiation were measured on whole cores using the MST. Thermal conductivity was measured on each core, using the whole core where possible. After core splitting, undrained shear strength, index properties, and additional measurements of *P*-wave velocity were conducted on the working half.

Multisensor Track Measurements

The MST, which is described in detail by Blum (1997), consists of four sensors: the magnetic susceptibility logger, gamma ray attenuation densiometer (GRA), *P*-wave logger (PWL), and natural gamma ray detector (NGR). MST data were sampled at discrete intervals along the core. The sample interval and the data acquisition period for each sensor were set to optimize the resolution of data acquired within the sampling time available for each core. MST data are significantly degraded if the core liner is only partially filled or if the core is disturbed. When RCB or XCB drilling was used, the core diameter was less than the nominal 6.6-cm core diameter. The reduced core diameter required corrections of the

values measured by the MST. The values in the database do not reflect these corrections, but the figures presented in the following chapters show corrected data.

Magnetic Susceptibility Logger

Magnetic susceptibility is the degree to which a material can be magnetized by an external magnetic field. If the ratio of magnetic susceptibility is expressed per unit of volume, volume susceptibility is defined as

$$\kappa = M/H,$$

where M = the volume magnetization induced in a material of susceptibility (κ) by the applied external field (H). Volume susceptibility is a dimensionless quantity. It can be used to help detect changes in magnetic properties caused by variations in lithology or by alteration. Magnetic susceptibility was measured at 5-cm intervals along the core using a Bartington meter (model MS2C) with an 88-mm coil diameter and a 2-s integration period. The Bartington meter operates at a frequency of 0.565 kHz and creates a field intensity of 80 A/m (= 0.1 mT), significantly lower than the field intensity needed to change the field orientation of magnetite grains (~50 mT). The width of the instrument response to a thin layer of material with a high magnetic susceptibility is ~10 cm. For this reason, the first and last measurement of each core section was taken 4 cm from the core section ends.

Gamma Ray Attenuation Densiometer

The GRA densiometer estimates bulk density by measuring the attenuation of gamma rays traveling through the core from a ^{137}Cs source. The gamma rays are attenuated by Compton scattering as they pass through the sample. The transmission of gamma rays through the sample is related to the electron density of the sample by

$$Y_t = Y_i \times e^{-nsd},$$

where

Y_t = the transmitted flux,
Y_i = the incident flux on a scatterer of thickness d,
n = the number of scatterers per unit volume or the electron density, and
s = the cross-sectional area per electron.

The bulk density (ρ) of the material is related to the electron density (n) by

$$n = \rho \times N_{AV} \times (Z/A),$$

where

Z = the atomic number or number of electrons,
A = the atomic mass of the material, and
N_{AV} = Avogadro's number.

Bulk density estimates are therefore accurate as long as the ratio Z/A of the constituent elements is approximately constant and corresponds to the ratio Z/A of the calibration standard. The GRA densiometer was calibrated to a standard consisting of varying amounts of water and aluminum so that the densities of sediments can be accurately determined. GRA density was measured using a 2-s integration period at 5-cm intervals along the core.

Compressional Wave (*P*-Wave) Logger

The compressional wave (*P*-wave) logger (PWL) measures the ultrasonic traveltime of a 500-kHz compressional wave pulse through the core and the core liner. A pair of displacement transducers monitors the separation between the *P*-wave transducers, and the distance is used to convert ultrasonic traveltime into velocity after correcting for the liner. Good coupling between the liner and the core is crucial to obtaining reliable measurements. The PWL is calibrated by placing a water core between the transducers. The PWL was set to take the mean of 1000 velocity measurements over a 2-s period at 5-cm intervals along the core.

Natural Gamma Ray Detector

The NGR measures the discrete decay of ^{40}K, ^{232}Th, and ^{238}U, three long-period isotopes that decay at essentially constant rates within measurable timescales. Minerals that include K, Th, and U are the primary source of natural gamma rays. These minerals are found in clays, arkosic silts and sandstones, potassium salts, bituminous and alunitic schists, phosphates, certain carbonates, some coals, and acid or intermediate igneous rocks (Serra, 1984). The operation of the NGR is outlined by Hoppie et al. (1994). The NGR system contains four scintillation counters arranged at 90° angles from each other in a plane orthogonal to the core track. The counters contain doped sodium iodide crystals and photomultipliers to produce countable pulses. The total response curve of the instrument is estimated to be ~40 cm and so integrates a relatively long length of core in comparison to the other instruments of the MST. Natural gamma ray emissions were measured over a 20-s period at 10-cm intervals. The NGR was calibrated in port against a thorium source and during Leg 195 by measuring sample standards at the end of operations at every site.

Thermal Conductivity

Thermal conductivity is the measure of the rate at which heat flows through a material. It is dependent on the composition, porosity, density, and structure of the material. Thermal conductivity profiles of sediments and rock sections are used, along with temperature measurements, to estimate heat flow. Thermal conductivity is measured through the transient heating of a core sample with a known geometry using a known heat source and recording the change in temperature with time, using the TK04 system described by Blum (1997). For soft sediment, thermal conductivity measurements are made using a needle probe (Von Herzen and Maxwell, 1959) on whole-core sections; the reported value is the mean of three repeated measurements. For materials too hard for the needle probe to penetrate, thermal conductivity measurements are made after core splitting, using the needle probe in a half-space configuration (Vacquier, 1985); the reported value is the

mean of four repeated measurements. Thermal conductivity measurements were made at an interval of at least one per core unless variations in lithology required more frequent sampling.

Undrained Shear Strength

The undrained and residual shear strength of sediments and serpentinite mud was measured using a Wykeham-Farrance motorized vane shear apparatus following procedures described by Boyce (1977). In making vane shear measurements, it is assumed that a cylinder of sediment is uniformly sheared around the axis of the vane in an undrained condition. The vane used for all measurements has a 1:1 length to diameter blade ratio with a dimension of 1.28 cm. A high vane rotation rate of 90°/min was used to minimize pore fluid expulsion while measurements take place. Torque and strain measurements at the vane shaft were made using a torque transducer and potentiometer. Undrained shear strength measurements were made at least once per core section unless variations in lithology required more frequent sampling.

P-Wave Velocity

Discrete *P*-wave velocity measurements were made in three directions in the sediments using two pairs of insertion transducers (PWS1 and PWS2) with fixed separations of 7 and 3.5 cm, respectively, and a pair of contact transducers (PWS3) in a modified Hamilton Frame. PWS1, PWS2, and PWS3 use a 500-kHz compressional wave pulse to measure ultrasonic traveltimes, which, when combined with transducer separation data, can be used to determine velocity. PWS1 and PWS2 were only used to measure velocity in soft sediments, where they were inserted into the face of the split core. PWS1 is aligned with the core axis (the z-direction), and PWS2 is aligned perpendicular to the core axis (the y-direction). PWS3 is mounted vertically with one transducer fixed and the other mounted onto a screw, allowing the transducer separation to be altered. PWS3 measures velocity in the x-direction in split cores but is also used to measure velocity in discrete samples of hard sediments or crystalline rock. Distilled water is applied to PWS3 to improve the acoustic coupling between the transducers and the sample. *P*-wave velocity measurements were made at least once per core section.

Index Properties Measurements

Minicore samples of ~10 cm³ were collected using a piston sampler in soft sediment or an electric drill in rocks. Samples were taken at least once per section. Sediment samples were placed in a 20-mL beaker and sealed to prevent moisture loss. Rock samples were soaked in seawater for 24 hr before determining the wet mass. Samples were then dried in an oven at 105° ± 5°C for 24 hr and allowed to cool in a desiccator before measuring dry weights and volumes (method C in Blum, 1997). Wet and dry sample masses and dry volumes were measured and used to calculate wet bulk density, dry density, grain density, water content, and porosity. Sample mass was determined using two Scientech electronic balances. The balances are equipped with a computerized averaging system that corrects for ship accelerations. The sample mass is counterbalanced by a known mass such that the mass differentials are generally <1 g. Sample volumes were measured at least three times, or until a consistent reading was obtained, using a helium-displacement

Quantachrome penta-pycnometer. A standard reference volume was included with each group of samples during the measurements and rotated among the cells to check for instrument drift and systematic error; each time an error was detected in the measurement of the reference volume, the offending cell was calibrated. The following relationships can be computed from the two mass measurements and dry volume measurements (taken from Blum, 1997, pp. 2-2 to 2-3). When a beaker is used, its mass and volume are subtracted from the measured total mass and volume. This results in the following directly measured values:

M_b (bulk mass),
M_d (dry mass)   = mass of solids (M_s) + mass of residual salt, and
V_d (dry volume) = volume of solids (V_s) + volume of evaporated salt (V_{salt}).

Variations in pore water salinity (s) and density (ρ_{pw}) that typically occur in marine sediments do not affect the calculations significantly, and standard seawater values under laboratory conditions are used:

s   = 0.035 wt% and
ρ_{pw} = 1.024 g/cm^3.

Pore water mass (M_{pw}), mass of solids (M_s), and pore water volume (V_{pw}) can then be calculated:

$$M_{pw} = (M_b - M_d)/(1-s),$$

$$M_s = M_b - M_{pw} = (M_d - [s \times M_b])/(1-s), \text{ and}$$

$$V_{pw} = M_{pw}/\rho_{pw} = (M_b - M_d)/[(1-s)\times\rho_{pw}].$$

Additional parameters required are the mass and volume of salt (M_{salt} and V_{salt}, respectively) to account for the phase change of pore water salt during drying. It should be kept in mind that for practical purposes, the mass of salt is the same in solution and as a precipitate, whereas the volume of salt in solution is negligible. Thus,

$$M_{salt} = M_{pw} - (M_b - M_d) = [(M_b - M_d) \times s]/(1-s), \text{ and}$$

$$V_{salt} = M_{salt}/\rho_{salt} = \{[(M_b - M_d) \times s]/(1-s)\}/\rho_{salt},$$

where the salt density ($\rho_{salt} = 2.20$ g/cm^3) is a calculated value for average seawater salt.

Moisture content is the pore water mass expressed either as percentage of wet bulk mass or as a percentage of the mass of salt-corrected solids:

$$W_b = M_{pw}/M_b = (M_b - M_d)/[M_b \times (1-s)], \text{ and}$$

$$W_s = M_{pw}/M_s = (M_b - M_d)/[M_d - (s \times M_b)].$$

Calculations of the volume of solids and bulk volume are as follows:

$$V_s = V_d - V_{salt} \text{ and}$$

$$V_b = V_s + V_{pw}.$$

Bulk density (ρ_b), density of solids or grain density (ρ_s), dry density (ρ_d), porosity (P), and void ratio (e) are then calculated according to the following equations:

$$\rho_b = M_b/V_b,$$

$$\rho_s = M_s/V_s,$$

$$\rho_d = M_s/V_b,$$

$$P = V_{pw}/V_b, \text{ and}$$

$$e = V_{pw}/V_s.$$

Electrical Resistivity and Formation Factor

The electrical resistivity of the sediment was measured using a four-electrode configuration. The instrument used was modified at the University of California, Santa Cruz, from the design of Andrews and Bennett (1981) and was built at the University of Hawaii. The electrodes consisted of four stainless steel pins that are 2 mm in diameter, 15 mm in length, and spaced 13 mm apart. A 20-kHz square-wave current was applied on the outer electrodes, and the difference in potential between the two inner electrodes was measured. The size of the current (typically 50 mA) was measured over a resistor in the outer circuit.

The main purpose of measuring sediment resistivity was to determine the formation factor, defined as the ratio of the resistivity of sediment with included pore water divided by the resistivity of the pore water alone. In practice, the formation factor is approximated by measuring the apparent resistivity of the sediment in the split core liner and dividing that value by the apparent resistivity of seawater of similar salinity and the same temperature in a 30-cm length of split core liner. Using the same configuration for the measurement of the apparent resistivities removes the effects of geometry from the determination of the formation factor.

Hydraulic Conductivity and Specific Storage

The hydraulic conductivity and specific storage of the serpentinite mud was measured during a consolidation test. In this test, an axial surface load is applied to a laterally constrained sample. The axial load produces an excess pore fluid pressure along the length of the core. The bottom of the sample is drained so that the excess pore fluid pressure at that point is zero. The loads and boundary conditions are applied by a Manheim squeezer, and the amount of fluid displaced is measured as a function of time. Figure F10 is a cartoon of the apparatus and the boundary conditions. Also shown is the pressure profile along the length of the sample at various times. The assumption of incompressible mineral grains and water, common to soil mechanics (Wang, 2000), allows the volume of water discharged from the sample to be converted to axial displacement using the cross-sectional area of the sample. Be-

F10. Experimental apparatus, boundary conditions, and pore pressure profiles, p. 50.
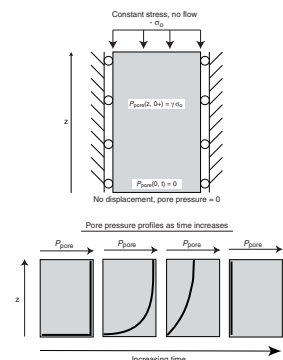
cause the frame, not the mineral grains or the water, is compressed, we can calculate the axial displacement using the following equation:

Δw = volume of water discharged/cross-sectional area of sample,

where Δw = the axial displacement. We then use the relationship for displacement in an infinite length cylinder as a function of time (Wang, 2000):

$$\Delta w(t) = 2c_m \gamma \sigma_z \sqrt{\frac{Dt}{\pi}},$$

to determine the lumped product of constants (on the right hand side of the following equation) by plotting the slope of the displacement over the square root of time

$$\frac{\Delta w}{\sqrt{t}} = 2c_m \gamma \sigma_z \sqrt{\frac{D}{\pi}},$$

where

c_m = the vertical compressibility,
γ = the loading efficiency,
σ_z = the axial load, and
D = the hydraulic diffusivity.

Figure **F11** compares experimentally determined displacements with calculated displacements as a function of time. Only the early time portion of the plot is used to determine the lumped product of constants. Early in the experiment, the decrease in pore pressure has not yet diffused to the end of the sample and so the approximation of an infinite cylinder is still valid. To determine the hydraulic diffusivity (D) from the lumped product, we need to determine the other unknown factors, c_m and γ.

The vertical compressibility is defined by

$$c_m \equiv \frac{\left(\frac{\Delta w}{w_o}\right)}{\Delta \sigma_z}\Bigg|_{err = 0}.$$

Because all the components of the equation above, axial displacement (Δw), axial stress (σ_z), and sample length (w_o) are measured, it is possible to calculate the vertical compressibility. Also, because the pore pressure throughout the entire length of the sample returns to zero at very long times, the boundary condition of no change in pore pressure ($\Delta P_{pore} = 0$) is met.

The loading efficiency is defined as

$$\gamma \equiv \frac{\Delta P_{pore}}{\Delta \sigma_z}\Bigg|_{err = 0},$$

where P_{pore} = the pore fluid pressure. The assumption of incompressible grains and pore fluid leads to a value = 1 (Wang, 2000).

The specific storage (S_s) is related to the vertical compressibility under the assumptions of incompressible grains and pore fluid by

$$S_s = c_m \times \rho_f \times g,$$

F11. Comparison of the calculated displacements to measured displacements as a function of time, p. 51.
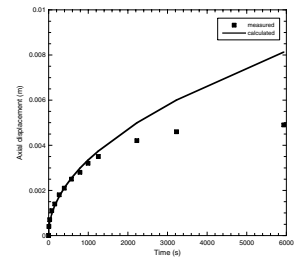
where

ρ_f = the fluid density, and
g = the acceleration of gravity.

Finally, we can determine the hydraulic conductivity from the hydraulic diffusivity and specific storage using

$$K = D \times S_s.$$

DOWNHOLE MEASUREMENTS

Downhole logs are spatially continuous records of the in situ physical, chemical, and structural properties of the formation penetrated by a borehole. The logs are recorded rapidly using a variety of probes combined into tool strings. These strings are lowered downhole on a heave-compensated electrical wireline and pulled up at a constant speed to provide continuous simultaneous measurements of the various properties as a function of depth. Logs can be used to interpret the stratigraphy, lithology, mineralogy, and geochemical composition of the penetrated formation. Where core recovery is incomplete or disturbed, log data may provide the only way to characterize the borehole section. Where core recovery is good, log and core data complement one another and may be interpreted jointly. Downhole logs are also sensitive to formation properties on a scale that is intermediate between laboratory measurements on core samples and geophysical surveys. The logs are used to calibrate the interpretation of geophysical survey data, for example, through the use of synthetic seismograms and to provide a necessary link for the integrated understanding of physical properties on all scales.

Two standard ODP logging tool strings were deployed during Leg 195: the triple combination (triple combo), and the Formation Micro-Scanner (FMS)/sonic combination. In addition to wireline logs, in situ temperature measurements were made with the Adara tool, which is located in the coring shoe of the APC during piston-coring operations, and the Davis-Villinger temperature probe, which is deployed on a wireline in between retrieval of RCB cores.

Logging Tools

The tool strings used during Leg 195 were as follows:

1. The triple combo (porosity, density, and resistivity) tool string (Fig. F12), which consists of the accelerator porosity sonde (APS), the hostile-environment lithodensity sonde (HLDS), and either the dual laterolog (DLL) or the phasor dual induction–spherically focused resistivity tool (DIT-E), depending on formation resistivity. The hostile-environment natural gamma sonde (HNGS) is included at the top of the string and the Lamont-Doherty Earth Observatory (LDEO) temperature/acceleration/pressure tool (TAP) at the bottom.
2. The FMS/sonic tool string (Fig. F12), which consists of the FMS, the general purpose inclinometer tool (GPIT), and a sonic sonde. Because of a malfunction during the previous leg, the dipole shear sonic imager (DSI), which is normally used, was replaced

F12. Triple combo and Formation MicroScanner/sonic tool strings, p. 52.
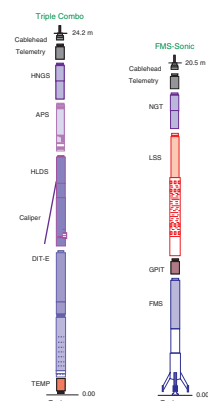
by the long-spaced sonic sonde (LSS). The natural gamma ray tool (NGT) was included at the top of this tool string.

Each tool string includes a telemetry cartridge, for communicating through the wireline with the downhole logging laboratory on the drillship, and a natural gamma ray sonde, which is used to identify lithologic markers, providing a common reference for correlation and depth shifting between multiple logging runs. Logging runs are typically conducted at 250–275 m/hr.

The logging tools are briefly described below, and their operating principles, applications, and approximate vertical resolution are summarized in Table **T2.** Some of the principal data channels of the tools, their physical significance, and units of measure are listed in Table **T3.** More detailed information on individual tools and their geological applications may be found in Ellis (1987), Goldberg (1997), Lovell et al. (1998), Rider (1996), Schlumberger (1989, 1994), Serra (1984, 1986, 1989), and the Lamont-Doherty Earth Observatory Borehole Research Group (LDEO-BRG) Guide to ODP Wireline Logging Services CD (2001) or on the World Wide Web at **http://www.ldeo.columbia.edu/BRG/ ODP/LOGGING/MANUAL/index.html.**

T2. Logging tools and their applications, p. 55.

T3. Principal data channels generated by logging tools, p. 56.

Natural Radioactivity

Two spectral gamma ray tools were used to measure and classify natural radioactivity in the formation: the HNGS and the NGT. The NGT uses a sodium iodide scintillation detector and five-window spectroscopy to determine concentrations of K (in weight percent), Th (in parts per million), and U (in parts per million), the three elements whose isotopes dominate the natural gamma radiation spectrum. The NGT response is sensitive to borehole diameter and the weight and concentration of bentonite or KCl present in the drilling mud; these effects are routinely corrected for during processing at LDEO. The HNGS is similar to the NGT, but it uses two bismuth germanate scintillation detectors for significantly improved tool precision. Spectral analysis in the HNGS filters out gamma ray energies below 500 keV, eliminating sensitivity to bentonite or KCl in the drilling mud and improving measurement accuracy.

Density

Formation density was determined from the density of electrons in the formation, which was measured with the HLDS. The sonde contains a radioactive cesium (^{137}Cs) gamma ray source (622 keV) and far and near gamma ray detectors mounted on a shielded skid, which is pressed against the borehole wall by a hydraulically activated arm. Gamma rays emitted by the source undergo Compton scattering, which involves the transfer of energy from gamma rays to electrons in the formation via elastic collision. The number of scattered gamma rays that reach the detectors is directly related to the number of electrons in the formation, which is in turn related to bulk density. Porosity may also be derived from this bulk density if the matrix density is known.

The HLDS also measures the photoelectric effect factor (PEF) caused by absorption of low-energy gamma rays. Photoelectric absorption occurs when the energy of the gamma rays drops below 150 keV after being repeatedly scattered by electrons in the formation. As the PEF depends on the atomic number of the elements in the formation, it varies

according to chemical composition and is essentially independent of porosity. For example, the PEF of pure calcite = 5.08, illite = 3.03, quartz = 1.81, and kaolinite = 1.49 b/e⁻. PEF values can be used in combination with NGT curves to identify different types of clay minerals. Coupling between the tool and the borehole wall is essential for good HLDS logs. Poor contact results in underestimation of density values. The radius of investigation into the formation of the lithodensity tool is on the order of tens of centimeters, depending on the density of the rock.

Porosity

Formation porosity was measured with the APS. The sonde incorporates a minitron neutron generator, which produces fast (14.4 MeV) neutrons, and five neutron detectors (four epithermal and one thermal) located at different spacings from the source. The tool is pressed against the borehole wall by an eccentralizing bow-spring. Emitted neutrons are slowed down by collisions. The amount of energy lost per collision depends on the relative mass of the nucleus with which the neutron collides. The greatest energy loss occurs when the neutron strikes a nucleus nearly equal to its own mass, such as hydrogen, which is mainly present in the pore water. The neutron detectors record both the numbers of neutrons arriving at various distances from the source and the neutron arrival times, which act as a measure of formation porosity. However, as hydrogen bound in minerals such as clays or in hydrocarbons also contributes to the measurement, the raw porosity value is often an overestimate.

Electrical Resistivity

Two tools were used to measure the formation electrical resistivity: the DIT-E and the DLL. The DIT-E provides three measurements of electrical resistivity, each with a different depth of investigation into the formation. Deep- and medium-penetration measurements are made inductively using transmitter coils that are energized with high-frequency alternating currents, creating time-varying magnetic fields that induce secondary Foucault currents in the formation. The strength of these induced ground currents is inversely proportional to the resistivity of the formation through which they circulate, as are the secondary inductive fields that they create. The amplitude and phase of the secondary magnetic fields, measured with receiving coils, are used as a proxy for the formation resistivity. Shallow penetration measurements with a high vertical resolution are made with a spherically focused laterolog. This measures the current necessary to maintain a constant voltage drop across a small fixed interval. Because of the inductive nature of the deep- and medium-penetration measurements, DIT-E logs are accurate only for formations with resistivities less than ~100 Ωm, such as sediments. In more resistive formations, the measurement error becomes significant (>20%) and it is more suitable to use the DLL (Schlumberger, 1989).

The DLL provides two measures of formation electrical resistivity, labeled "deep" (LLd) and "shallow" (LLs) on the basis of their respective depths of investigation. In both devices, a current beam, 61 cm thick, is forced horizontally into the formation using focusing (also called bucking) currents. For the deep measurement, both focusing and measurement currents return to a remote electrode on the surface; thus, the depth of investigation is considerable, and the effects from borehole

conductivity and adjacent formations are reduced. In the shallow laterolog, the return electrodes that measure the bucking currents are located on the sonde and, therefore, the current sheet retains focus over a shorter distance than the deep laterolog. Fracture porosity can be estimated from the separation between the deep and shallow measurements, based on the observation that the former is sensitive to the presence of horizontal conductive fractures only, whereas the latter responds to both horizontal and vertical conductive structures. The DLL has a response range of 0.2–40,000 Ωm.

The depth of investigation of both the DIT-E and the DLL depends on the resistivity of the rock and on the resistivity contrast between the zone invaded by drilling fluid and the uninvaded zone. In formations with resistivities >100 Ωm, the average radial depth of investigation of the DIT-E is ~1.5 m for the deep induction phasor-processed resistivity, 76 cm for the medium induction phasor-processed resistivity, and 38 cm for the spherically focused resistivity log. These values drop by ~20% for a 0.1-Ωm formation resistivity. The depth of investigation of the DLL will vary with the separation between the sonde and the remote current return at the surface.

In most rocks, electrical conduction occurs primarily by ion transport through pore fluids and is strongly dependent on porosity. Electrical resistivity data can therefore be used to estimate formation porosity using Archie's Law (Archie, 1942) if the formation does not contain clay. Archie's Law is expressed as

$$FF = a\phi^{-m},$$

where

- FF = the formation factor (i.e., the ratio of the formation resistivity to that of the pore fluids),
- ϕ = the porosity,
- m = the cementation factor, dependent on the tortuosity and connectivity of pore spaces, and
- a = a constant that varies with rock type.

For a first-order interpretation, conventionally, $a = 1$ and $m = 2$, but more rigorous values can be determined from resistivity and porosity measurements on core samples (see **"Physical Properties,"** p. 19).

The DIT-E also measures spontaneous potential (SP) fields. Spontaneous potentials can originate from a variety of causes: electrochemical, electrothermal, electrokinetic streaming potentials, and membrane potentials due to differences in the mobility of ions in the pore and drilling fluids. The interpretation of SP logs remains problematic because of this multiplicity of sources.

Temperature, Acceleration, and Pressure

Downhole temperature, acceleration, and pressure were measured with the LDEO high-resolution TAP tool. When attached to the bottom of the triple combo tool string, the TAP is run in an autonomous mode with data stored in built-in memory. Two thermistors are mounted near the bottom of the tool to detect borehole fluid temperatures at different rates. A thin, fast-response thermistor is able to detect small, abrupt changes in temperature. A thicker, slow-response thermistor is used to

estimate temperature gradients and thermal regimes more accurately. The pressure transducer is included to activate the tool at a specified depth. A three-axis accelerometer measures tool movement downhole, providing data for analyzing the effects of heave on a deployed tool string, which should eventually lead to the fine tuning of the wireline heave compensator (WHC).

The borehole temperature record provides information on the thermal regime of the surrounding formation. The vertical heat flow can be estimated from the vertical temperature gradient combined with measurements of the thermal conductivity from core samples. The temperature record must be interpreted with caution, as the amount of time elapsed between the end of drilling and the logging operation is generally not sufficient to allow the borehole to recover thermally from the influence of drilling fluid circulation. The data recorded under such circumstances may differ significantly from the equilibrium temperature of that environment. Nevertheless, from the spatial temperature gradient, it is possible to identify abrupt temperature changes that may represent localized fluid flow into the borehole, indicative of fluid pathways and fracturing and/or breaks in the temperature gradient that may correspond to contrasts in permeability at lithologic boundaries.

Acoustic Velocity

The DSI, which is conventionally used on the FMS/sonic string, was not functional during Leg 195, and the LSS was used to measure the elastic compressional wave velocity of the formation. The LSS provides long-spacing measurements through the "depth derived" borehole compensation principle. Acoustic traveltime readings between two acoustic sources, spaced 2 ft apart, and two receivers, also spaced 2 ft apart, are memorized at one depth and combined with a second set of readings made after the sonde has been pulled an appropriate distance up the borehole. The LSS records the full waveform for each source-receiver pair, in addition to its automatic determination of arrival time. The radial depth of investigation for sonic tools depends on the spacing of the detectors and on the petrophysical characteristics of the rock, such as rock type, porosity, and alteration, but is of the order of tens of centimeters. Velocity data, together with the formation density data, can be used to generate a synthetic seismogram.

Formation MicroScanner

The FMS provides high-resolution electrical resistivity–based images of borehole walls, which can be used for detailed lithologic or structural interpretation. The tool has four orthogonal arms (pads), each containing 16 microelectrodes, or "buttons," which are pressed against the borehole wall during recording (Fig. F13). The electrodes are arranged in two diagonally offset rows of eight electrodes each and are spaced ~2.5 mm apart (Fig. F13). A focused current is emitted from the four pads into the formation, with a return electrode near the top of the tool. Array buttons on each of the pads measure current intensity variations in the formation. Processing transforms these measurements, which reflect microresistivity variations in the formation into continuous, spatially oriented, high-resolution images that mimic geologic structures behind the borehole walls. FMS images are oriented with respect to magnetic north using the GPIT. This allows further processing that can provide measurements of dip amount and dip direction (azi-

F13. Schematic diagram showing the FMS tool downhole, p. 53.
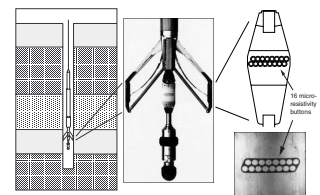
muth) of planar features in the formation. FMS images are particularly useful for mapping structural features, dip determination, detailed core-log correlation, positioning of core sections with poor recovery, and analysis of depositional environments. For example, FMS images have been used for identifying sedimentation patterns in turbidite deposits (Lovell et al., 1998), facies changes (Serra, 1989), and volcanic stratigraphy (Brewer et al., 1998).

The FMS image is sensitive to structure within a radial depth of ~25 cm from the borehole wall and has a vertical resolution of 5 mm with coverage of ~22% of the borehole wall on a given pass. FMS logging commonly includes two passes, the images of which can be merged to improve borehole wall coverage. To produce reliable FMS images, the pads must be firmly pressed against the borehole wall. The maximum extension of the caliper arms is 15.0 in. In holes with a diameter >15 in, the pad contact will be inconsistent and the FMS images can be blurred. The maximum borehole deviation for which good data can be recorded with this tool is 10°. Irregular borehole walls will also adversely affect the images, as contact with the wall is poor.

Magnetic Field Measurement

Downhole magnetic field measurements were made with the GPIT. The primary purpose of this sonde, which incorporates a three-component accelerometer and a three-component magnetometer, is to determine the acceleration and orientation of the FMS/sonic tool string during logging. The acceleration data allow more precise determination of log depths than is possible on the basis of cable length alone, as the wireline is subject to both stretching and ship heave. Acceleration data are also used in processing of FMS data to correct the images for irregular tool motion.

Local magnetic anomalies, generated by high remanent magnetization of the basalts in the basement section of a borehole, can interfere with the determination of tool orientation. However, these magnetic anomalies can be useful for inferring the magnetic stratigraphy of the basement section.

Log Data Quality

The quality of log data may be seriously degraded if the hole diameter is excessively large or changes rapidly. Resistivity and velocity measurements are the least sensitive to borehole effects, whereas the nuclear measurements (density, neutron porosity, and both natural and induced spectral gamma rays) are most sensitive because of the large attenuation by borehole fluid. Corrections can be applied to the original data to reduce the effects of these conditions and, generally, any departure from the conditions under which the tool was calibrated.

Logs from different tool strings may have depth mismatches, caused by either cable stretch or ship heave during recording. Small errors in depth matching can distort the logging results in zones of rapidly changing lithology. To minimize the effects of ship heave, a hydraulic WHC adjusts for rig motion during logging operations. Distinctive features recorded by the NGT, run on every tool string, provide correlation and relative depth offsets among the logging runs and can be calibrated to distinctive lithologic contacts observed in the core recovery or drilling penetration (e.g., basement contacts). Precise core-log depth matching is difficult in zones where core recovery is low because of the inher-

ent ambiguity of placing the recovered section within the cored interval. The precision and reliability of the various logging measurements are governed by the resolutions of the various tools and the condition of the drill hole. The vertical resolution of the various logging tools is generally ~46 cm, with several exceptions (Table T2).

In Situ Temperature Measurements

Temperature measurements were taken at Site 1200 during Leg 195 to determine the in situ temperatures within the conduit of the serpentine mud volcano. The discrete in situ measurements were made with the Adara tool, which is located in the coring shoe of the APC during piston-coring operations. The components of the tool include a platinum temperature sensor and a data logger. The platinum resistance-temperature device is calibrated for temperatures ranging from –20° to 100°C, with a resolution of 0.01°C. In operation, the adapted coring shoe is mounted on a regular APC core barrel and lowered down the pipe by wireline. The tool is typically held for 5–10 min at the mudline to equilibrate with bottom-water temperatures and then is lowered to the bottom of the drill string. Standard APC coring techniques are used, with the core barrel being fired out through the drill bit using hydraulic pressure. The Adara tool (and the APC corer) remains in the sediment for 10–15 min to obtain a temperature record. This provides a sufficiently long transient record for reliable extrapolation back to the steady-state temperature. The nominal accuracy of the temperature measurement is ~0.1°C.

Data Recording and Processing

Data for each logging run were recorded, stored digitally, and monitored in real time using the Schlumberger MAXIS 500 system. After logging at each hole, data were transferred to the shipboard downhole measurements laboratory for preliminary processing and interpretation. FMS image data were processed and interpreted using Schlumberger's GeoFrame 3.7 software package. Logs from the shipboard processed data were plotted as depth-related curves or images representing the physical and chemical properties of the strata penetrated.

Log data were also transmitted to LDEO-BRG using a FFASTEST satellite high-speed data link for further processing soon after each hole was logged. Data processing at LDEO-BRG includes (1) depth-shifting all logs relative to a common datum (i.e., meters below seafloor), (2) corrections specific to individual tools, and (3) quality control and rejection of unrealistic or spurious values. Once processed at LDEO-BRG, log data were transmitted back to the ship, providing near real-time data processing. Log curves of LDEO-BRG processed data were then replotted on board for refining interpretations (see "Downhole Measurements" sections in each site chapter). Further postcruise processing of the log data from the FMS is performed at LDEO-BRG.

Postcruise, processed acoustic, caliper, density, gamma ray, magnetic, neutron porosity, resistivity, and temperature data in ASCII format are available directly from the LDEO-BRG World Wide Web site at **http://www.ldeo.columbia.edu/BRG/ODP/DATABASE/DATA/search.html.** Access to logging data is restricted to Leg 195 participants for 12 months following the completion of the leg, and a password is required to access data during this period. Thereafter, access to these log data is

free. A summary of "logging highlights" is also posted on the LDEO-BRG web site at the end of each leg.

Downhole logging aboard *JOIDES Resolution* is provided by LDEO-BRG in conjunction with Leicester University Borehole Research, the Laboratoire de Mesures en Forage (Université de Montpellier 2), University of Aachen, University of Tokyo, and Schlumberger Well Logging Services.

MICROBIOLOGY

The primary microbiological objective at Site 1200 was to estimate the microbial community structure and phylogenetic diversity from core samples derived from a natural window (i.e., South Chamorro Seamount) into the ultradeep subsurface biosphere. The approach was to use molecular biological techniques to assess the degree of commonality and uniqueness among different microbial taxa originating from these communities, by taking advantage of small-subunit ribosomal deoxyribonucleic acids (SSU rDNAs) as discriminators for categorizing multiple microbial populations (community structure) and as descriptors of a single microbial population's ancestry (phylogeny). We also planned to correlate these molecular phylogeny results with variations in pore water geochemistry to interpret the metabolic potential of the most dominant microbial populations. Our goal during these comparisons was to test our hypothesis that these microbial taxa are the residual survivors of ultradeep subsurface conditions and mud volcanism mass transport encountered in the Mariana subduction system.

To achieve these objectives, samples from RCB and APC cores from Site 1200 were collected for both shipboard and shore-based studies.

Shipboard studies and preservation procedures included

1. Determination of the abundance and distribution of microorganisms by direct counting fluorescence microscopy, along with morphological characterizations by light microscopy;
2. The preservation of subsamples for molecular biological analyses by quick freezing with liquid nitrogen and then maintenance at –70°C until transport to shore-based laboratories on dry ice;
3. The preservation of subsamples in 2.5% glutaraldehyde for scanning electron microscopy (SEM) and, potentially, transmission electron microscopy (TEM) preparations, stored at –20°C;
4. The preservation of subsamples for fluorescent in situ hybridization probing, first for 2–3 hr at a final concentration of 3.0% (w/v) paraformaldehyde (in phosphate buffered saline [PBS], 10-mM sodium phosphate, 138-mM NaCl [pH = 7.4]), washed twice with $1 \times$ PBS, and finally, stored in $1 \times$ PBS:ethanol solution (1:1) at –20°C;
5. The aseptic cryopreservation of subsamples placed in 30% glycerol solution and quick freezing in liquid nitrogen for use with multiple enrichment culture procedures; and
6. The preservation of subsamples in serum vials stored at 4°C under nitrogen-flushed headspace for use in enrichment cultures under various conditions (thermal and aerobic/anaerobic).

Sampling and preservation was conducted in order to carry out the following shore-based studies:

1. Molecular biological assays, including amplified ribosomal DNA restriction analysis as a means of determining the initial community structure from both the bacterial and archaeal components of the microbial community (Moyer, 2001);
2. Sequencing of the SSU rDNAs from the most dominant community members to allow for a molecular phylogeny analysis so that evolutionary relationships and potential physiological characteristics can be inferred (Moyer, 2001);
3. High-throughput community tracking with terminal-restriction fragment length polymorphism to examine the spacial distribution of predetermined marker populations across an array of core samples (Marsh et al., 2000);
4. Fluorescent in situ hybridization and/or other staining procedures to determine the role of microorganisms in these respective communities (Ravenschlag et al., 2001);
5. SEM techniques and/or TEM studies to further examine sediment-microbial interaction processes;
6. Lipid extraction and analysis to determine total viable biomass, community structure, and metabolic status using phospholipid fatty acid analysis; and
7. Anaerobic and aerobic enrichment culturing of targeted populations after the preliminary interpretation of initial molecular biological assays.

Interpretation of shipboard and shore-based results is complicated by the possibility of contamination of samples with microbes from seawater, drilling equipment, and postcollection processing of samples. To minimize the problems of contamination, special handling, sampling, and sample treatment protocols were established.

Shipboard Sampling

Whole-round cores or large fragments of the core were collected immediately after the core reached the catwalk and after the core liner was split. Whole rounds were broken away from the rest of the core to minimize the potential for cross contamination by cutting. The cores were handled only with nitrile gloves. Following selection of an appropriate piece, the whole-round sample was transferred to the laminar flow hood in the microbiology lab, where the outside of the sample was stripped away using a flamed (sterilized) spatula. Subsequently, the subsamples were processed and preserved, usually within 20–30 min of the core arriving on deck.

Tracer Tests

To confirm the suitability of the core material for microbiological research, contamination assays were conducted to quantify the intrusion of drill water using in situ pore water chemistry (e.g., chlorinity) (see "Geochemistry," p. 17), and fluorescent microspheres were used as particulate tracers (Smith et al., 2000a, 2000b). These tests were carried out on either the same or an adjacent 10-cm whole-round sample.

Shipboard Studies

The abundance of subsurface microorganisms was determined by direct fluorescence microscopic counting after acridine orange staining.

Such observations give a first-order approximation of the extent of the deep subsurface biosphere. For direct counting, small sediment samples (0.1–0.2 cm^3) were diluted in 1.0 mL of filtered (0.2 µm), sterilized PBS. After this solution was vortexed vigorously, 50 µL was removed with a wide-bore aerosol-resistant pipet tip and diluted in 1.0 mL of PBS. Samples were mixed thoroughly before removing an aliquot for filtration on preblacked polycarbonate filters (Isopore, Millipore; pore size = 0.2 µm; diameter = 25 mm). The filters were stained with a filtered (0.2 µm) acridine orange (0.025% [w/v] final concentration in PBS). The cells on the filters were examined with a Zeiss fluorescence microscope at 400–2000× magnification (100× Plan-Neofluar objective) using epifluorescence illumination (100-W Hg bulb) with ultraviolet and blue filters set for acridine orange. Cells were enumerated and normalized to the volume filtered.

REFERENCES

Andrews, D., and Bennett, A., 1981. Measurements of diffusivity near the sediment-water interface with a fine-scale resistivity probe. *Geochim. Cosmochim. Acta,* 45:2169–2175.

Archie, G.E., 1942. The electrical resistivity log as an aid in determining some reservoir characteristics. *J. Pet. Technol.,* 5:1–8.

Balsam, W.L., and Damuth, J.E., 2000. Further investigations of shipboard vs. shore-based spectral data: implications for interpreting Leg 164 sediment composition. *In* Paull, C.K., Matsumoto, R., Wallace, P., and Dillon, W.P. (Eds.), *Proc. ODP, Sci. Results,* 164: College Station, TX (Ocean Drilling Program), 313–324.

Balsam, W.L., Damuth, J.E., and Schneider, R.R., 1997. Comparison of shipboard vs. shore-based spectral data from Amazon-Fan Cores: implications for interpreting sediment composition. *In* Flood, R.D., Piper, D.J.W., Klaus, A., and Peterson, L.C. (Eds.), *Proc. ODP, Sci. Results,* 155: College Station, TX (Ocean Drilling Program), 193–215.

Balsam, W.L., Deaton, B.C., and Damuth, J.E., 1998. The effects of water content on diffuse reflectance measurements of deep-sea core samples: an example from ODP Leg 164 sediments. *Mar. Geol.,* 149:177–189.

—————, 1999. Evaluating optical lightness as a proxy for carbonate content in marine sediment cores. *Mar. Geol.,* 161:141–153.

Barnes, R.O., 1988. ODP in-situ fluid sampling and measurement: a new wireline tool. *In* Mascle, A., Moore, J.C., et al., *Proc. ODP, Init. Repts.,* 110: College Station, TX (Ocean Drilling Program), 55–63.

Berggren, W.A., Hilgen, F.J., Langereis, C.G., Kent, D.V., Obradovich, J.D., Raffi, I., Raymo, M.E., and Shackleton, N.J., 1995a. Late Neogene chronology: new perspectives in high-resolution stratigraphy. *Geol. Soc. Am. Bull.,* 107:1272–1287.

Berggren, W.A., Kent, D.V., Swisher, C.C., III, and Aubry, M.-P., 1995b. A revised Cenozoic geochronology and chronostratigraphy. *In* Berggren, W.A., Kent, D.V., Aubry, M.-P., and Hardenbol, J. (Eds.), *Geochronology, Time Scales and Global Stratigraphic Correlation.* Spec. Publ.—Soc. Econ. Paleontol. Mineral., 54:129–212.

Blum, P., 1997. Physical properties handbook: a guide to the shipboard measurement of physical properties of deep-sea cores. *ODP Tech. Note,* 26 [Online]. Available from World Wide Web: <http://www-odp.tamu.edu/publications/tnotes/tn26/INDEX.HTM>. [Cited 2001-03-02]

Boyce, R.E., 1977. Deep Sea Drilling Project procedures for shear strength measurement of clayey sediment using modified Wykeham Farrance laboratory vane apparatus. *In* Barker, P.F., Dalziel, I.W.D., et al., *Init. Repts. DSDP,* 36: Washington (U.S. Govt. Printing Office), 1059–1068.

Brewer, T.S., Harvey, P.K., Lovell, M.A., Haggas, S., Williamson, G., and Pezard, P., 1998. Ocean floor volcanism: constraints from the integration of core and downhole logging measurements. *In* Harvey, P.K., and Lovell, M.A. (Eds.), *Core-Log Integration,* Spec. Publ.—Geol. Soc. London, 136:341–362.

Cande, S.C., and Kent, D.V., 1995. Revised calibration of the geomagnetic polarity timescale for the Late Cretaceous and Cenozoic. *J. Geophys. Res.,* 100:6093–6095.

Ellis, D.V., 1987. *Well Logging for Earth Scientists:* New York (Elsevier).

Gieskes, J.M., Gamo, T., and Brumsack, H., 1991. Chemical methods for interstitial water analysis aboard *JOIDES Resolution. ODP Tech. Note,* 15.

Goldberg, D., 1997. The role of downhole measurements in marine geology and geophysics. *Rev. Geophys.,* 35:315–342.

Hoppie, B.W., Blum, P., and the Shipboard Scientific Party, 1994. Natural gamma-ray measurements on ODP cores: introduction to procedures with examples from Leg 150. *In* Mountain, G.S., Miller, K.G., Blum, P., et al., *Proc. ODP, Init. Repts.,* 150: College Station, TX (Ocean Drilling Program), 51–59.

Lamont-Doherty Earth Observatory Borehole Research Group, 2001. *Guide to ODP Wireline Logging Services CD:* Lamont-Doherty Earth Observatory–Borehole Research Group.

Lourens, L.J., Antonarakou, A., Hilgen, F.J., Van Hoof, A.A.M., Vergnaud-Grazzini, C., and Zachariasse, W.J., 1996. Evaluation of the Plio-Pleistocene astronomical timescale. *Paleoceanography,* 11:391–413.

Lovell, M.A., Harvey, P.K., Brewer, T.S., Williams, C., Jackson, P.D., and Williamson, G., 1998. Application of FMS images in the Ocean Drilling Program: an overview. *In* Cramp, A., MacLeod, C.J., Lee, S.V., and Jones, E.J.W. (Eds.), *Geological Evolution of Ocean Basins: Results from the Ocean Drilling Program.* Spec. Publ.—Geol. Soc. London, 131:287–303.

Manheim, F.T., and Sayles, F.L., 1974. Composition and origin of interstitial waters of marine sediments, based on deep sea drill cores. *In* Goldberg, E.D. (Ed.), *The Sea* (Vol. 5): *Marine Chemistry: The Sedimentary Cycle:* New York (Wiley), 527–568.

Marsh, T.L., Saxman, P., Cole, J., and Tiedje, J., 2000. Terminal restriction fragment length polymorphism analysis program, a web-based research tool for microbial analysis. *Appl. Environ. Microbiol.,* 66:3616–3620.

Martini, E., and Müller, C., 1986. Current Tertiary and Quaternary calcareous nannoplankton stratigraphy and correlations. *Newsl. Stratigr.,* 16:99–112.

Mazzullo, J.M., Meyer, A., and Kidd, R.B., 1988. New sediment classification scheme for the Ocean Drilling Program. *In* Mazzullo, J., and Graham, A.G. (Eds.), *Handbook for Shipboard Sedimentologists.* ODP Tech. Note, 8:45–67.

McKee, E.D., and Weir, G.W., 1953. Terminology for stratification and cross-stratification in sedimentary rocks. *Geol. Soc. Am. Bull.,* 64:381–390.

Moncrieff, A.C.M., 1989. Classification of poorly-sorted sedimentary rocks. *Sediment. Geol.,* 64:191–194.

Moyer, C.L., 2001. Molecular phylogeny: applications and implications for marine microbiology. *In* Paul, J.H. (Ed.), *Marine Microbiology:* San Diego (Academic Press), 375–394.

Munsell Color Company, Inc., 1975. *Munsell Soil Color Charts:* Baltimore, MD (Munsell).

Murray, R.W., Miller, D.J., and Kryc, K.A., 2000. Analysis of major and trace elements in rocks, sediments, and interstitial waters by inductively coupled plasma—atomic emission spectrometry (ICP-AES). *ODP Tech. Note,* 29 [Online]. Available from World Wide Web: <http://www-odp.tamu.edu/publications/tnotes/tn29/INDEX.HTM>. [Cited 2001-03-02]

Perch-Nielsen, K., 1985. Cenozoic calcareous nannofossils. *In* Bolli, H.M., Saunders, J.B., and Perch-Nielsen, K. (Eds.), *Plankton Stratigraphy:* Cambridge (Cambridge Univ. Press), 427–554.

Ravenschlag, K., Sahm, K., and Amann, R., 2001. Quantitative molecular analysis of the microbial community in marine arctic sediments (Svalbard). *Appl. Environ. Microbiol.,* 67:387–395.

Rider, M., 1996. *The Geological Interpretation of Well Logs* (2nd ed.): Caithness (Whittles Publishing).

Schlumberger, 1989. *Log Interpretation Principles/Applications:* Houston (Schlumberger Educ. Services), SMP–7017.

————, 1994. *IPL Integrated Porosity Lithology:* Houston (Schlumberger Wireline and Testing), SMP-9270.

Serra, O., 1984. *Fundamentals of Well-Log Interpretation* (Vol. 1): *The Acquisition of Logging Data:* Dev. Pet. Sci., 15A.

————, 1986. *Fundamentals of Well-Log Interpretation* (Vol. 2): *The Interpretation of Logging Data.* Dev. Pet. Sci., 15B.

————, 1989. *Formation MicroScanner Image Interpretation:* Houston (Schlumberger Educ. Services), SMP-7028.

Shepard, F., 1954. Nomenclature based on sand-silt-clay ratios. *J. Sediment. Petrol.,* 24:151–158.

Shipboard Scientific Party, 1987. Explanatory notes: ODP Leg 105, Baffin Bay and Labrador Sea. *In* Srivastava, S.P., Arthur, M., et al., *Proc. ODP, Init. Repts.,* 105: College Station, TX (Ocean Drilling Program), 21–42.

————, 1989. Introduction and explanatory notes. *In* Robinson, P.T., Von Herzen, R., et al., *Proc. ODP, Init. Repts.,* 118: College Station, TX (Ocean Drilling Program), 3–24.

————, 1990. Explanatory notes. *In* Fryer, P., Pearce, J.A., Stokking, L.B., et al., *Proc. ODP, Init. Repts.,* 125: College Station, TX (Ocean Drilling Program), 15–40.

————, 1995. Explanatory notes. *In* Flood, R.D., Piper, D.J.W., Klaus, A., et al., *Proc. ODP, Init. Repts.,* 155: College Station, TX (Ocean Drilling Program), 47–81.

————, 1999. Explanatory notes. *In* Dick, H.J.B., Natland, J.H., Miller, D.J., et al., *Proc. ODP, Init. Repts.,*176, 1–42 [CD-ROM]. Available from: Ocean Drilling Program, Texas A&M University, College Station, TX 77845-9547, U.S.A.

Smith, D.C., Spivack, A.J., Fisk, M.R., Haveman, S.A., Staudigel, H., and ODP Leg 185 Shipboard Scientific Party, 2000a. Methods for quantifying potential microbial contamination during deep ocean coring. *ODP Tech. Note,* 28 [Online]. Available from the World Wide Web: <http://www-odp.tamu.edu/publications/tnotes/tn28/INDEX.HTM>. [Cited 2001-03-02]

————, 2000b. Tracer-based estimates of drilling-induced microbial contamination of deep sea crust. *Geomicrobiol. J.,* 17:207–219.

Streckeisen, A., 1974. Classification and nomenclature of plutonic rocks. *Geol. Rundsch.,* 63:773–786.

Vacquier, V., 1985. The measurement of thermal conductivity of solids with a transient linear heat source on the plane surface of a poorly conducting body. *Earth Planet. Sci. Lett.,* 74:275–279.

Von Herzen, R.P., and Maxwell, A.E., 1959. The measurement of thermal conductivity of deep-sea sediments by a needle-probe method. *J. Geophys. Res.,* 64:1557–1563.

Wang, H.F., 2000. *Theory of Linear Poroelasticity with Applications to Geomechanics and Hydrogeology:* Princeton, N.J. (Princeton Univ. Press).

Wentworth, C.K., 1922. A scale of grade and class terms of clastic sediments. *J. Geol.,* 30:377–392.

Figure F1. Schematic examples of numbered core sections.
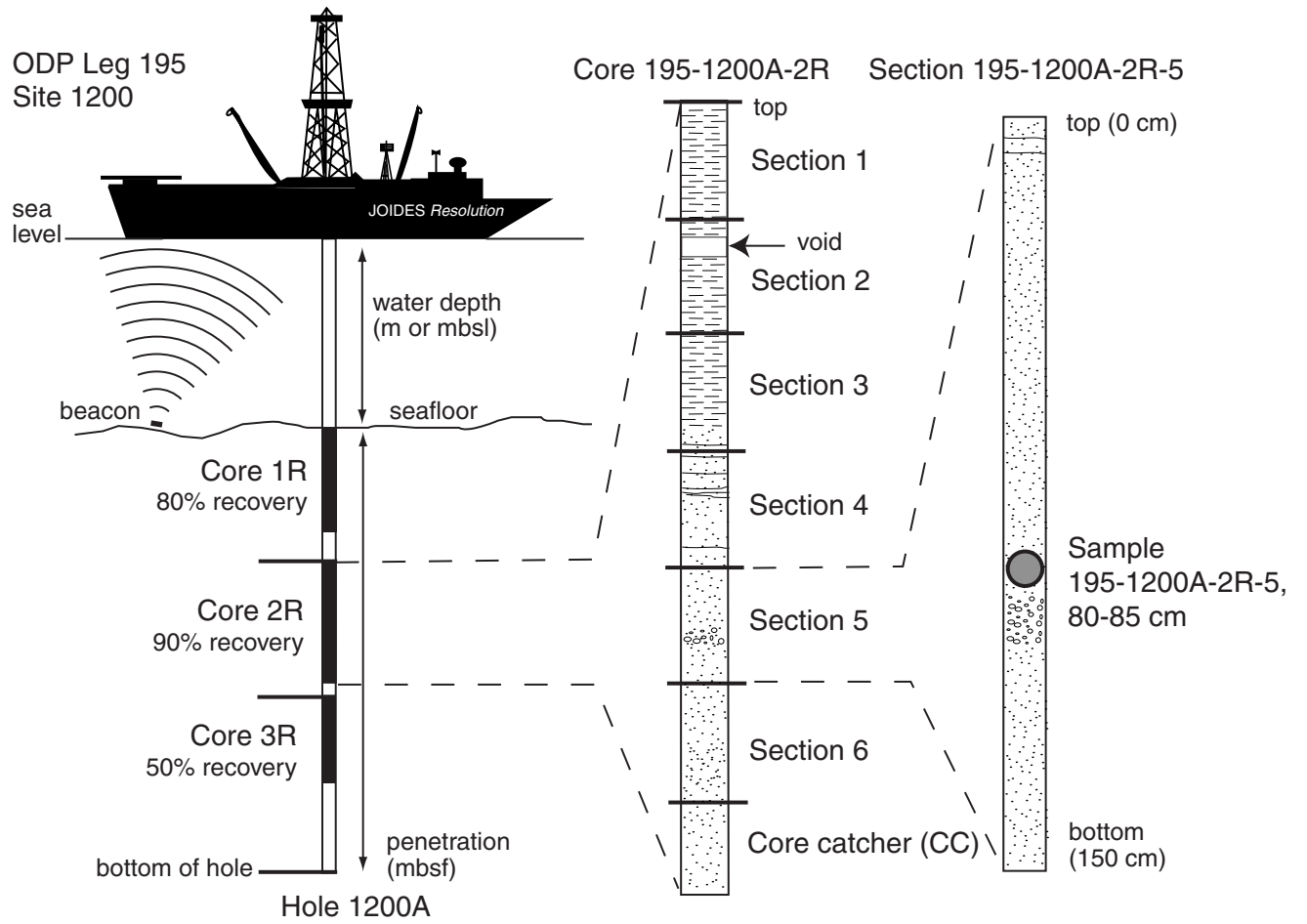
Figure F2. Textural classification scheme for siliciclastics, from Shepard (1954). Sand-, silt-, and clay-sized fractions are defined using the Wentworth (1922) grain-size scale. Numbers represent percent.
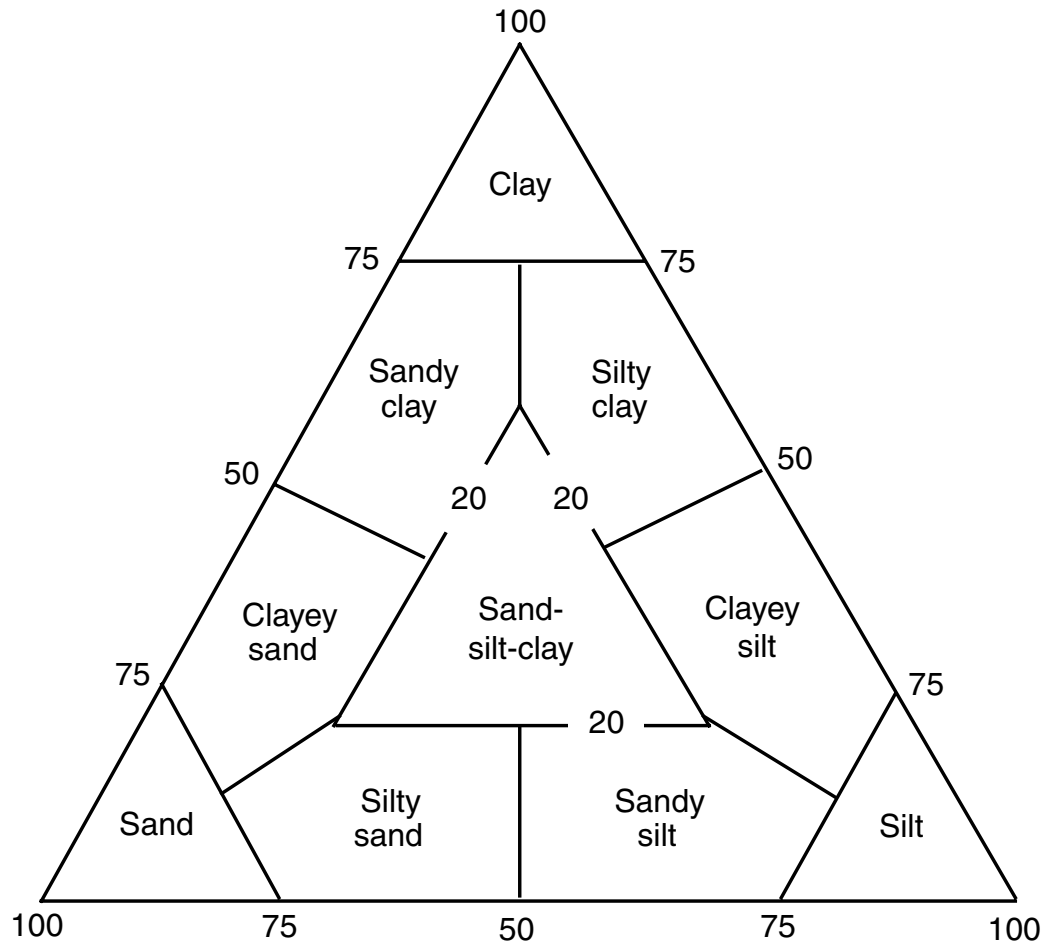
Figure F3. Classification of poorly sorted sediments with a gravel component to facilitate the characterization of diamicts, conglomerates, and breccias, modified after Moncrieff (1989). Matrix classification is based on Figure F2, p. 40, and should be inserted at the asterisk. The term "conglomerate" is used when clasts are rounded, the term "breccia" when clasts are angular.

		PERCENT GRAVEL (>2 MM) IN WHOLE ROCK ESTIMATED FROM CORE				
		Trace <5%	5%-10%	10%-30%	30%-80%	>80%
0 —	FINE-GRAINED SEDIMENTS	CLAY/SILT with dispersed clasts	CLAY/SILT with common clasts	CLAY/SILT with abundant clasts	clayey/silty CONGLOMERATE/ BRECCIA	CONGLOMERATE/ BRECCIA
25 —		* CLAY/SILT with dispersed clasts	Clast-poor * DIAMICT	Clast-rich * DIAMICT	* CONGLOMERATE/ BRECCIA	
50 —		* SAND with dispersed clasts	Clast-poor * DIAMICT	Clast-rich * DIAMICT	* CONGLOMERATE/ BRECCIA	
75 —		SAND with dispersed clasts	SAND with common clasts	SAND with abundant clasts	sandy CONGLOMERATE/ BRECCIA	
100 —						

Percent sand in matrix

* For matrix description see Fig. F2.

Figure F4. Key to symbols used to represent lithology, sedimentary structures, accessories, bioturbation, and drilling disturbance in AppleCORE barrel sheets, Leg 195. (Continued on next page).

LEGEND

Lithology
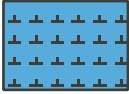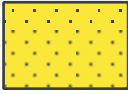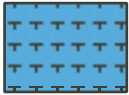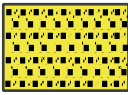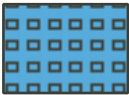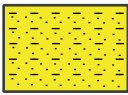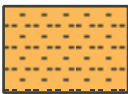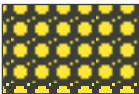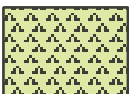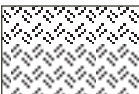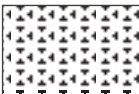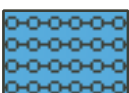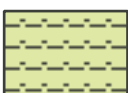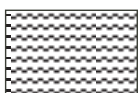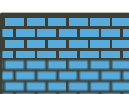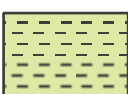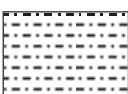
Nannofossil ooze	Sand/ Sandstone	Diamict/Diamictite with silt/clay matrix
Foraminifer ooze	Silty sand	Diamict/Diamictite with sandy matrix
Calcareous ooze	Clayey sand	Conglomerate
Diatom ooze	Silt/ Siltstone	Breccia
Radiolarian ooze	Sandy silt	Volcanic ash or tuff
Nannofossil chalk	Clayey silt	Volcanic lapilli
Foraminifer chalk	Clay/ Claystone	Volcanic breccia
Chalk	Sandy clay	Silt-sized, sand-sized serpentine
Limestone	Silty clay	Serpentine breccia
Chert	Sand-silt-clay	Sheared phacoidal serpentine

Figure F4 (continued).

Structures

⟋⟋	normal microfault
⟋	normal macrofault
⅃⊦	slickensides
⫽	reverse microfault
⟋	reverse macrofault
⌒⌒	current ripples
▪ ▪ ▪ ▪	isolated lamina
☰	planar lamination
⟋	flaser bedding
@	chaotic bedding
⫽ᴵ	cross lamination
⋯⋯	sand lamina
◌◌◌◌	pebbles/ granules/sand
▮	normal graded
▮	inverse graded
----	clay lamina
⋯⋯	silt lamina
▨	rock fragments
⊃	slump
⬭	lenticular bedding
⊟	calcite cement
⫽	mineral-filled fracture

Accessories

(Mn)	manganese concretion
Z	zeolite
⬤	lonestone
Py	pyrite
⬯	nodule
⬭	chert nodule
⟋	undefined burrow
⬚	fossil fragment
∂∂∂	shell fragments
▴▴	cherty
◤◥	rip-up clasts
⊏⊐	calcareous

Contacts

———	sharp
⁄⁄⁄⁄⁄	gradational
∿∿∿	scoured
⌇⌇⌇	bioturbated
∼∼∼	undulating
⊢⊢⊢	faulted
———	inclined

Bioturbation

▮	abundant
▮	common
▮	present
▮	rare

Drilling Disturbance

⦙	slightly disturbed
⦙	moderately disturbed
⟩	highly disturbed
⦂	soupy
⁝⁝	slurry
⟨	deformed
⅃	flow-in
⫽	fractured
⇝	highly fragmented
⊟	biscuits

Figure F5. Descriptive names for coherent lavas and intrusions.

Ideal combination: ④ + ③ + ② + ①

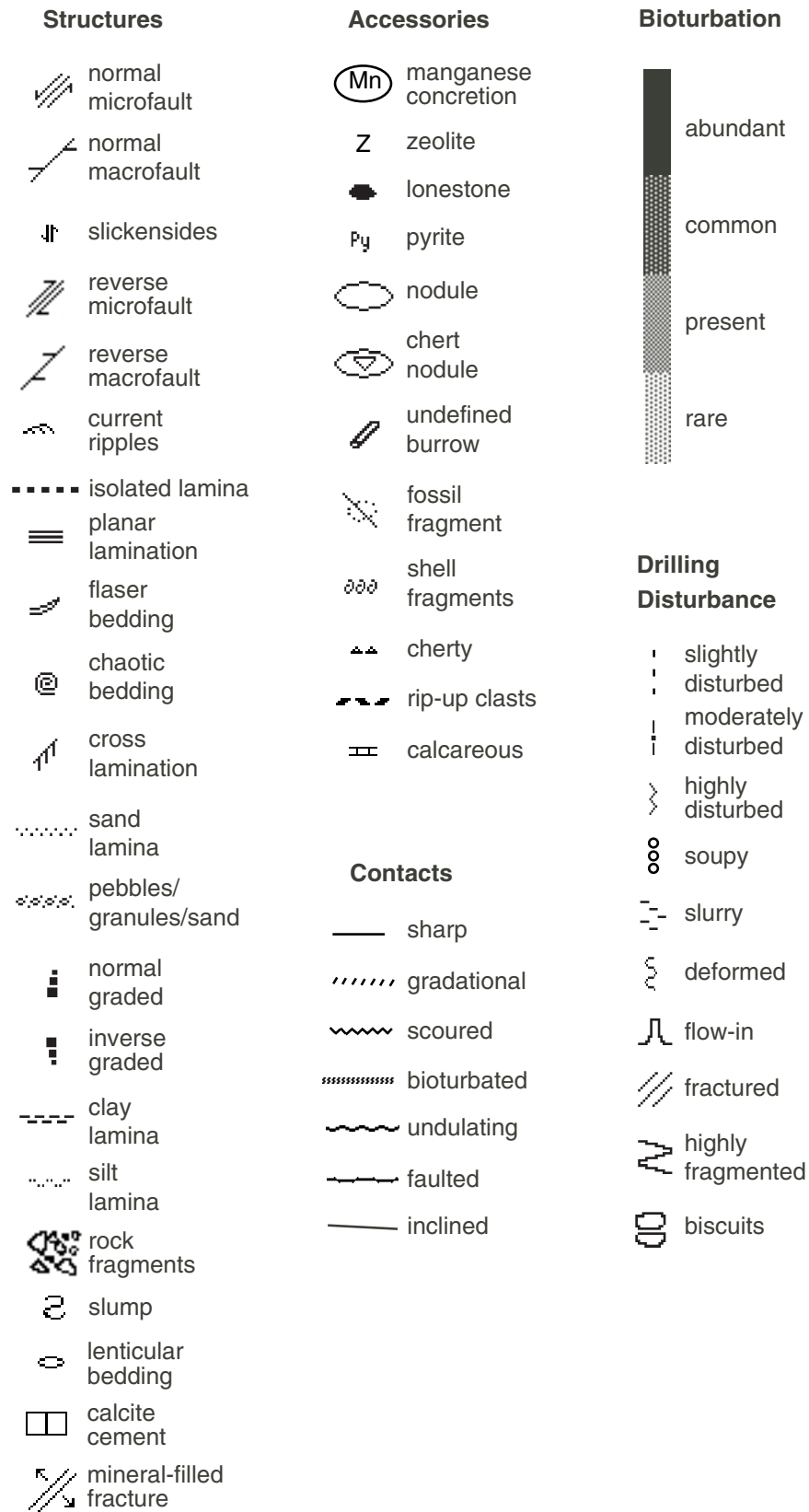alteration   texture   lithofacies term   composition

e.g., sericitic, highly quartz-phyric, coarse, flow-banded rhyolite; moderately vesicular, poorly olivine-phyric, fine, columnar jointed basalt

Minimum: ② + ①   e.g., blocky jointed rhyolite; massive basalt

③ + ①   e.g., hornblende-phyric andesite; aphanitic dacite(?)

④ + ①   e.g., sericite-silica rhyolite(?); chlorite-epidote andesite(?)

① COMPOSITION

a. estimate based on phenocryst assemblage
- rhyolite: K-feldspar ± quartz (± Ca-poor plagioclase ± ferromagnesian phase: biotite, amphibole, pyroxene, fayalite)
- dacite: plagioclase ± ferromagnesian phase: biotite, amphibole, pyroxene ± quartz (± K-feldspar)
- andesite: plagioclase ± ferromagnesian phase: biotite, amphibole, pyroxene (± olivine)
- basalt: pyroxene ± Ca-rich plagioclase ± olivine

b. for aphanitic samples, estimate based on color
- rhyolite(?), dacite(?): pale gray, pink, cream, pale green
- andesite(?), basalt(?): dark gray, dark blue, dark green, dark purple

② LITHOFACIES
- massive or flow-foliated, flow-banded, flow-laminated
- jointing: columnar, radial columnar, concentric, tortoise shell, blocky, prismatic, platy
- pillows or pseudo-pillows

③ TEXTURE
- porphyritic: a. phenocrysts — type (quartz-phyric, pyroxene-phyric, etc.)
  - abundance (poorly, moderately, highly)
  - size (fine ≤1 mm, medium 1-5 mm, coarse ≥5 mm)

  b. groundmass — glassy, cryptocrystalline, microcrystalline, very fine grained

- aphanitic: uniformly microcrystalline
- aphyric: no phenocrysts present
- glassy: composed of volcanic glass
- nonvesicular or vesicular (or amygdaloidal): sparsely ..., moderately ..., highly ..., pumiceous ..., scoriaceous ...
- spherulitic, microspherulitic, lithophysae-bearing

④ ALTERATION
- mineralogy: chlorite, sericite, silica, pyrite, carbonate, feldspar, hematite ...
- distribution: disseminated, nodular, spotted, pervasive, patchy ...

Figure F6. Spreadsheet for thin section description.

THIN SECTION:	20	195-1200A-13R-1,64-66 cm (Piece 7)				Unit 1		OBSERVER: IS, MD, MK
ROCK NAME:	Very highly altered serpentinite(after harzburgite)							
GRAIN SIZE:	Fine-grained							
TEXTURE:	Mesh, hourglass							

PRIMARY MINERALOGY	PERCENT PRESENT	PERCENT ORIGINAL	SIZE (mm) min.	max.	av.	APPROX. COMP.	MORPHOLOGY	COMMENTS
Olivine	20	83	0.01	0.2	0.05	Mg-rich	Anhedral	Sometimes strained.
Orthopyroxene	10	12	0.1	2	0.8	Mg-rich	Anhedral	Sometimes strained.
Clinopyroxene	<1	2				Mg-rich	Anhedral	
Amphibole								

OPAQUE MINERALS								
Magnetite	1						Dust-like	
Cr-spinel	2	3	0.05	0.8	0.4		Euhedral to embayed	
Sulfide								

SECONDARY MINERALOGY	PERCENT		SIZE (mm) min.	max.	av.		REPLACING / FILLING	COMMENTS
Antigorite								
Lizardite								
Chrysotile								
Serpentine	55				0.1		Olivine and orthopyroxene	
Brucite	10				0.05		Olivine and orthopyroxene	
Chlorite								
Talc								
Carbonate	2				0.05		Scattered	
Amphibole								
Clay minerals								

VEINS		LOCATION	min.	max.	av.		FILLING / MORPHOLOGY	COMMENTS
					0.3			

COMMENTS :	Few small veins

Figure F7. Classification diagram for mafic and ultramafic rock varieties (Streckeisen, 1974).
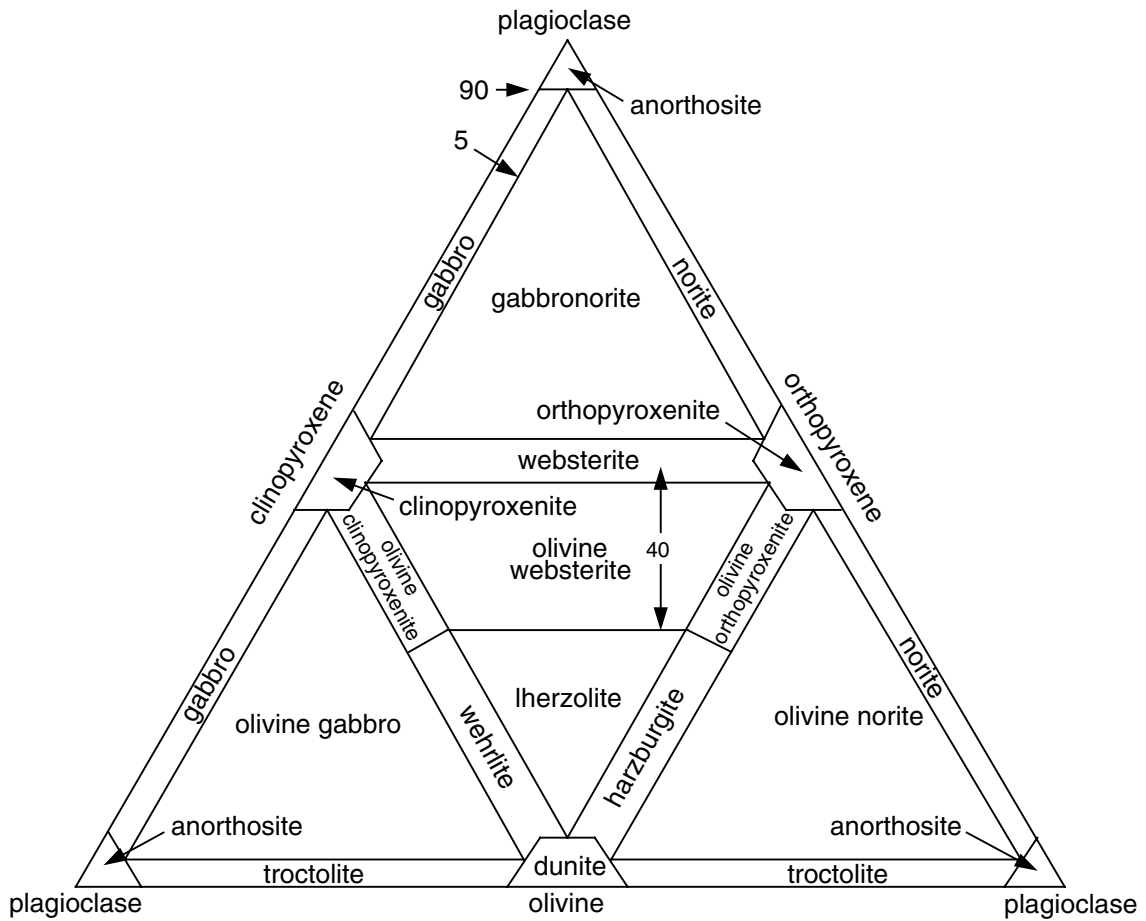
Figure F8. Streckeisen classification diagram for volcanic rocks (Streckeisen, 1974).
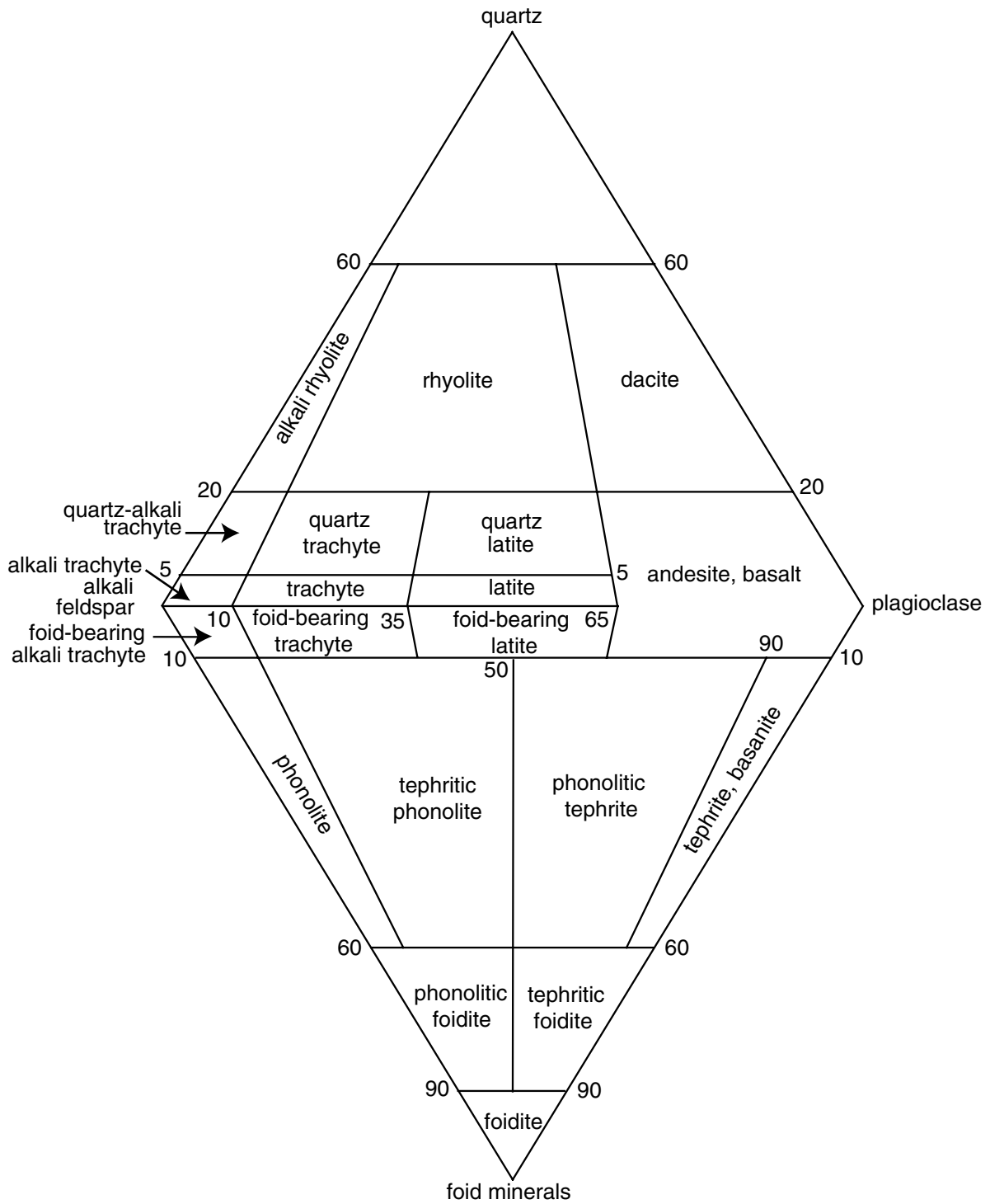
Figure F9. Nannofossil datums employed during Leg 195. The datums are after Berggren et al. (1995b); datums marked with an asterisk are after Berggren et al. (1995a). MPTS = magnetic polarity timescale, FO = first occurrence, LO = last occurrence. Polarity bands: black = normal, and white = reversed polarity. (Continued on next page.)
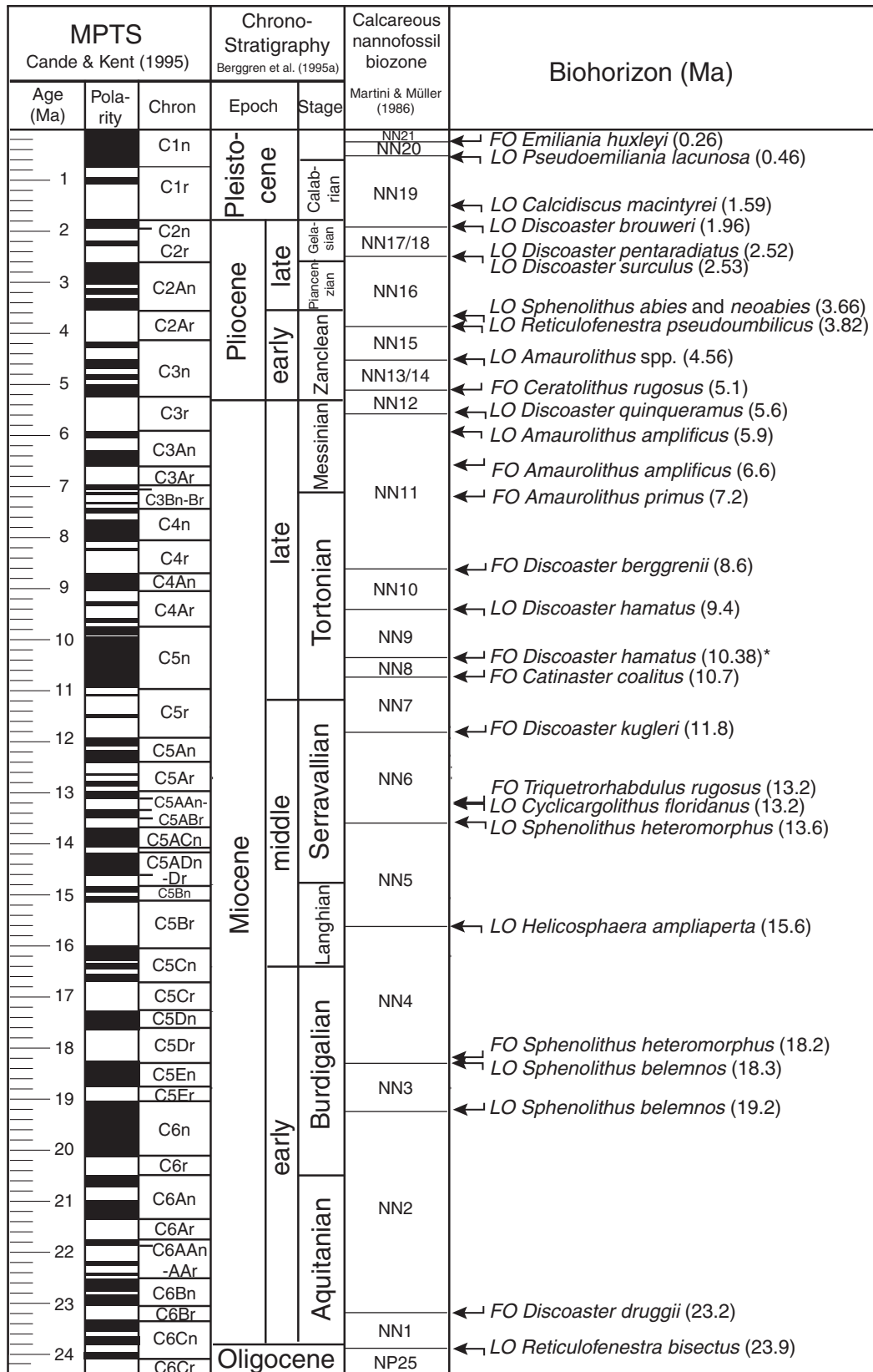

MPTS Cande & Kent (1995)			Chrono-Stratigraphy Berggren et al. (1995a)		Calcareous nannofossil biozone Martini & Müller (1986)	Biohorizon (Ma)
Age (Ma)	Pola-rity	Chron	Epoch	Stage		
		C1n	Pleistocene	Calabrian	NN21	FO Emiliania huxleyi (0.26)
					NN20	LO Pseudoemiliania lacunosa (0.46)
1		C1r			NN19	LO Calcidiscus macintyrei (1.59)
2		C2n	Pliocene	late	Gelasian	NN17/18	LO Discoaster brouweri (1.96)
		C2r				LO Discoaster pentaradiatus (2.52)
3		C2An			Piacenzian	NN16	LO Discoaster surculus (2.53)
4		C2Ar		early	Zanclean	NN15	LO Sphenolithus abies and neoabies (3.66)
							LO Reticulofenestra pseudoumbilicus (3.82)
5		C3n				NN13/14	LO Amaurolithus spp. (4.56)
						FO Ceratolithus rugosus (5.1)
6		C3r	Miocene	late	Messinian	NN12	LO Discoaster quinqueramus (5.6)
		C3An					LO Amaurolithus amplificus (5.9)
7		C3Ar				NN11	FO Amaurolithus amplificus (6.6)
		C3Bn-Br					FO Amaurolithus primus (7.2)
8		C4n			Tortonian		
		C4r					FO Discoaster berggrenii (8.6)
9		C4An				NN10	
		C4Ar					LO Discoaster hamatus (9.4)
10		C5n				NN9	
						NN8	FO Discoaster hamatus (10.38)*
11							FO Catinaster coalitus (10.7)
		C5r		middle	Serravallian	NN7	
12		C5An					FO Discoaster kugleri (11.8)
13		C5Ar				NN6	FO Triquetrorhabdulus rugosus (13.2)
		C5AAn-C5ABr					LO Cyclicargolithus floridanus (13.2)
14		C5ACn					LO Sphenolithus heteromorphus (13.6)
		C5ADn-Dr			Langhian	NN5	
15		C5Bn					
		C5Br					LO Helicosphaera ampliaperta (15.6)
16		C5Cn					
17		C5Cr		early	Burdigalian	NN4	
		C5Dn					
18		C5Dr					FO Sphenolithus heteromorphus (18.2)
		C5En				NN3	LO Sphenolithus belemnos (18.3)
19		C5Er					LO Sphenolithus belemnos (19.2)
		C6n					
20		C6r					
21		C6An			Aquitanian	NN2	
22		C6Ar					
		C6AAn-AAr					
		C6Bn					
23		C6Br					FO Discoaster druggii (23.2)
		C6Cn				NN1	
24		C6Cr	Oligocene			NP25	LO Reticulofenestra bisectus (23.9)

Figure F9 (continued).

Figure F10. Diagram of the experimental apparatus, boundary conditions, and pore pressure profiles with increasing time.

Constant stress, no flow

$- \sigma_o$

$P_{pore}(z, 0+) = \gamma \sigma_o$

$P_{pore}(0, t) = 0$

z

No displacement, pore pressure = 0

Pore pressure profiles as time increases

P_{pore} P_{pore} P_{pore} P_{pore}
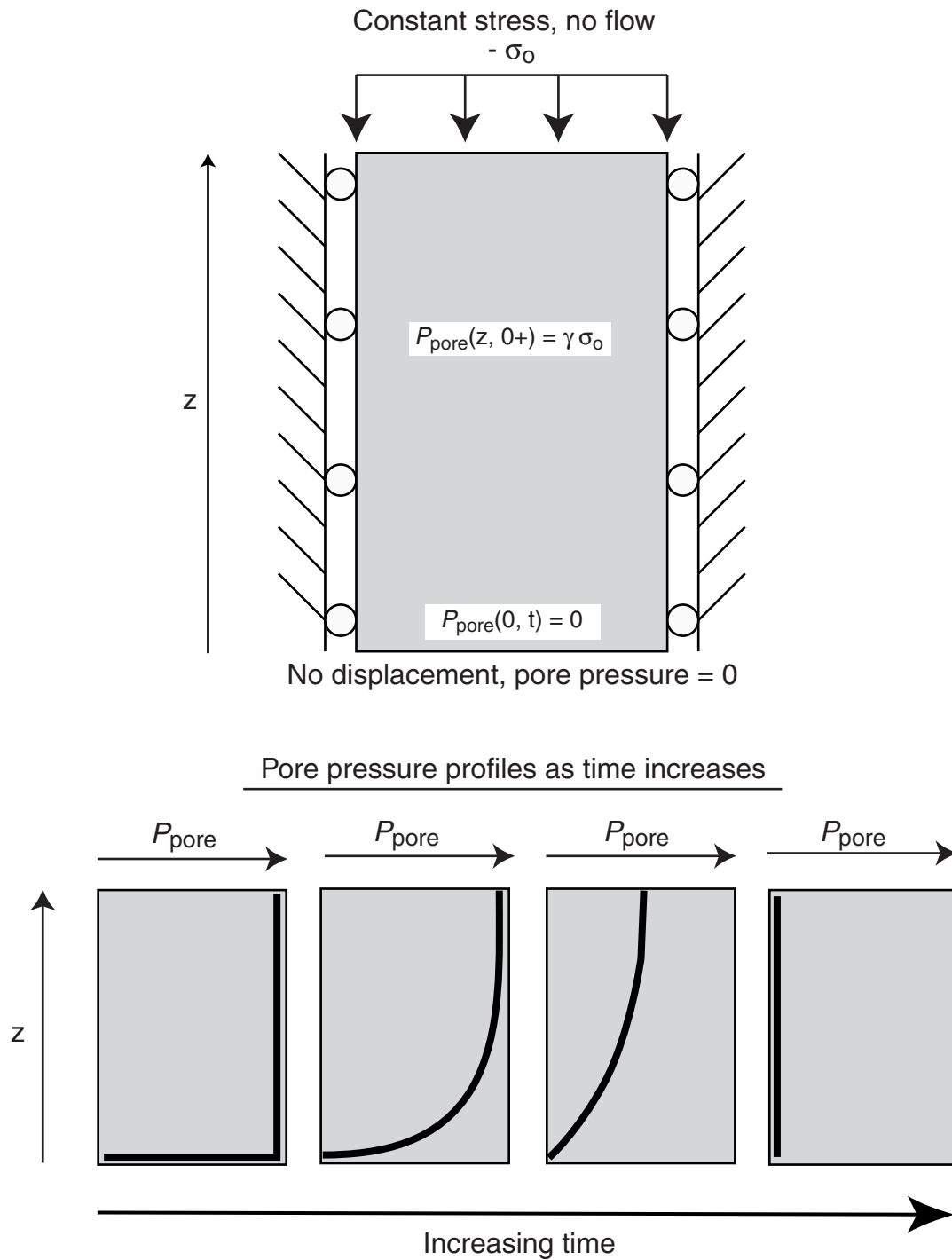
z

Increasing time

Figure F11. Comparison of the calculated displacements to measured displacements as a function of time. Note that at longer times the measured displacements approach an asymptotic value of displacement, whereas the calculated displacements will increase without bound.
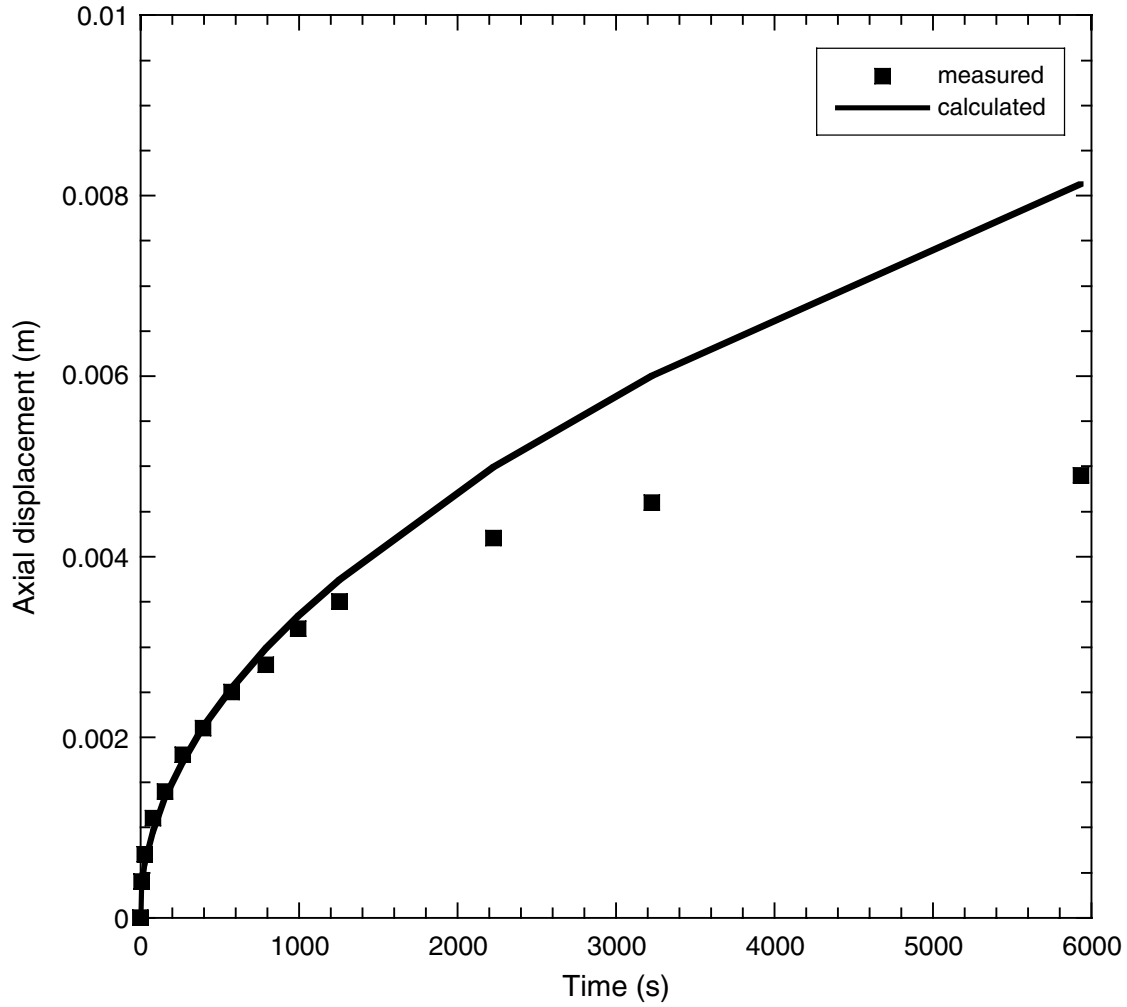
Figure F12. Triple combo and Formation MicroScanner/sonic tool strings used during Leg 195 (not to scale). HNGS = hostile-environment natural gamma sonde, APS = accelerator porosity sonde, HLDS = hostile-environment lithodensity sonde, DIT-E = phasor dual induction-spherically focused resistivity tool, TEMP = temperature probe, NGT = natural gamma spectrometry tool, LSS = long-spaced sonic sonde, GPIT = general purpose inclinometer tool, FMS = Formation MicroScanner.
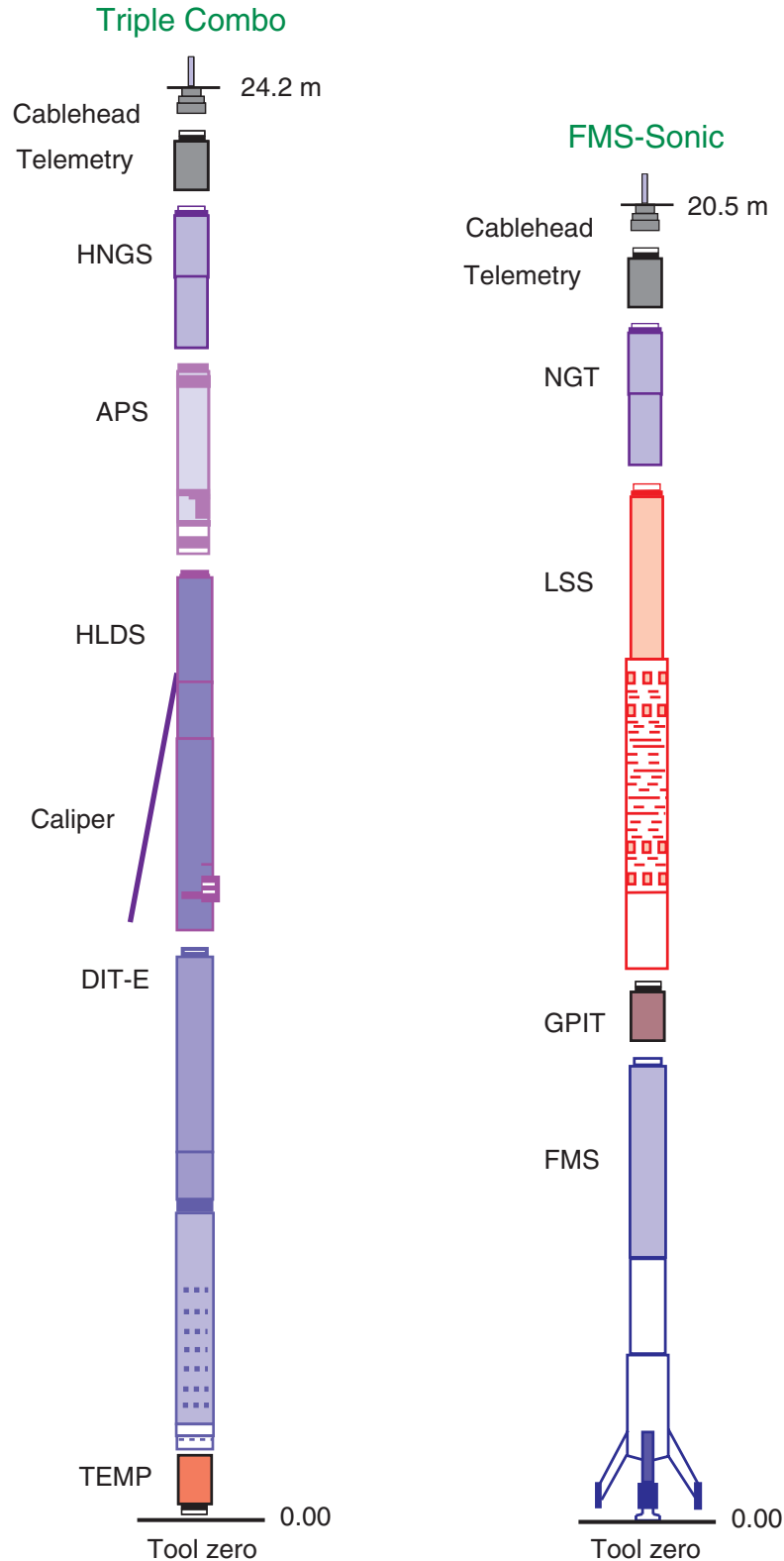
Figure F13. Schematic diagram showing the FMS tool downhole. The enlarged portion shows a photograph of the FMS caliper arms on which the microelectrode arrays are extended. The FMS electrode pad with 16 buttons used for microresistivity imaging of the borehole wall is also shown.

16 micro-
resistivity
buttons

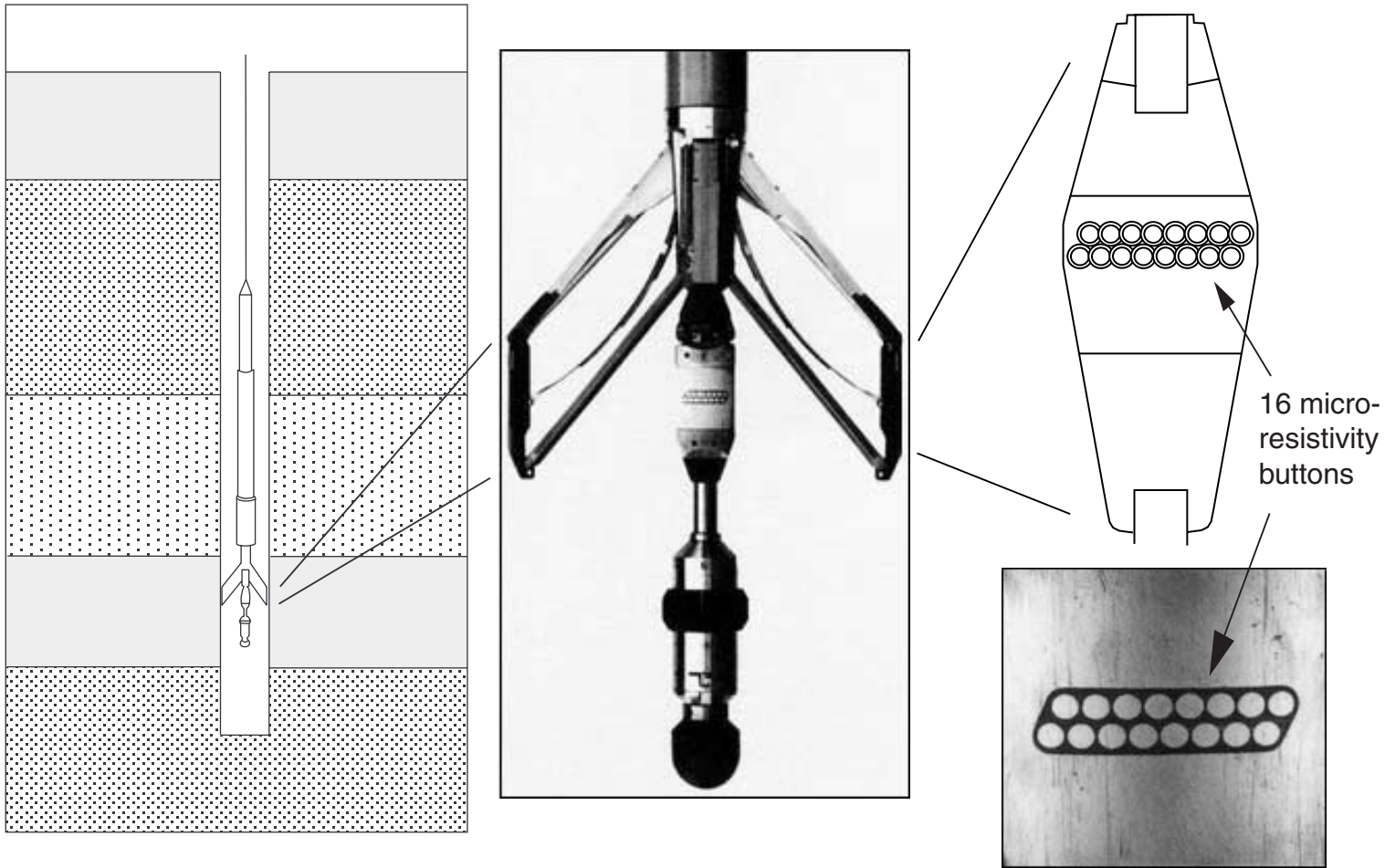**Table T1.** Detection limits for major and trace elements analyzed by inductively coupled plasma–atomic emission spectroscopy (ICP-AES).

Element	ICP-AES detection limit (ppb)
Al	28
Ba	1.3
Ca	0.2
Cr	7
Fe	6.2
K	60
Mg	1.6
Mn	1.4
Na	69
Ni	15
P	272
Sc	1.5
Si	12
Sr	0.4
Ti	3.8
V	7.5
Y	3.5
Zr	7.1

Table T2. Measurements made by wireline tool strings.

Run	Tool string*	Typical logging speed (m/hr)	Tools†	Measurement	Sample interval (cm)	Approximate vertical resolution (cm)
1	Triple combination (total length = ~36.05 m)	250–275	HNGS	Spectral gamma ray	15	51
			APS	Porosity	5 and 15	43
			HLDS	Bulk density, PEF	15	38
			DLL	Resistivity	15	61
			DIT-E	Resistivity	15	76–200
			TAP	Temperature	1 per s	NA
				Tool acceleration	4 per s	NA
				Pressure	1 per s	NA
2	Formation MicroScanner (FMS)/sonic combination (total length = ~33.4 m)	250–275	NGT	Spectral gamma ray	15	46
			GPIT	Tool orientation	0.25	NA
			LSS	Sonic velocity	15	61
			FMS	Microresistivity	0.25	0.5

Notes: * = all tool and tool string names except the TAP tool are trademarks of Schlumberger. † = for additional information about tool physics and use consult ODP Logging Services at **http://www.ldeo.columbia.edu/ BRG/ODP.** Tools: HNGS = hostile environment natural gamma ray sonde, APS = accelerator porosity sonde, HLDS = high-temperature lithodensity sonde, DLL = dual laterolog, DIT-E = dual induction tool, TAP = Lamont-Doherty temperature/acceleration/pressure tool, NGT = natural gamma spectrometry tool, GPIT = general purpose inclinometer tool, LSS = long-spaced sonic tool, FMS = Formation MicroScanner. PEF = photoelectric effect. NA = not applicable.

Table T3. Acronyms and units used for wireline tools.

Tool	Output	Explanation	Unit
APS		Accelerator porosity sonde	
	APLC	Near array porosity (limestone corrected)	%
	FPLC	Far array porosity (limestone corrected)	%
	SIGF	Formation capture cross section (Σ_f)	Capture units
	STOF	Tool standoff (computed distance from borehole wall)	in
DIT		Dual induction tool	
DLL		Dual laterolog	
	LLD	Deep resistivity	Ωm
	LLS	Shallow resistivity	Ωm
FMS		Formation MicroScanner	
GPIT		General purpose inclinometer tool	
	HAZI	Hole azimuth	Degrees
	FNOR	Intensity of the total magnetic field	oer
	F_x, F_y, F_z	Earth's magnetic field (three orthogonal directions)	Degrees
	A_x, A_y, A_z	Acceleration (three orthogonal directions)	m/s^2
HLDS		Hostile environment lithodensity sonde	
	RHOM	Bulk density (corrected)	g/cm^3
	PEFL	Photoelectric effect	b/e$^-$
	LCAL	Caliper (measure of borehole diameter)	in
	DRH	Bulk density correction	g/cm^3
HNGS		Hostile environment gamma ray sonde	
	HSGR	Standard (total) gamma ray	gAPI
	HCGR	Computed gamma ray (HSGR minus uranium contribution)	gAPI
	HFK	Potassium	wt%
	HTHO	Thorium	ppm
	HURA	Uranium	ppm
LSS		Long spacing sonic tool	
	V_p	Compressional wave velocity	ms/ft
NGT		Natural gamma ray spectrometry tool	
	SGR	Standard total gamma ray	gAPI
	CGR	Computed gamma ray (SGR minus uranium contribution)	gAPI
	POTA	Potassium	wt%
	THOR	Thorium	ppm
	URAN	Uranium	ppm
SFR		Spherically focused resistivity	
	IDPH	Deep induction phasor-processed resistivity	Ωm
	IMPH	Medium induction phasor-processed resistivity	Ωm
	SFLU	Shallow spherically focused resistivity	Ωm
TAP		Temperature/acceleration/pressure tool	°C, m/s^2, psi